Airborne cloud condensation nuclei measurements during the 2006 Texas Air Quality Study

Akua Asa-Awuku,[1,2] Richard H. Moore,[1] Athanasios Nenes,[1,3] Roya Bahreini,[4,5] John S. Holloway,[4,5] Charles A. Brock,[4] Ann M. Middlebrook,[4] Thomas B. Ryerson,[4] Jose L. Jimenez,[5,6] Peter F. DeCarlo,[5,6] Arsineh Hecobian,[3] Rodney J. Weber,[3] Robert Stickel,[3] Dave J. Tanner,[3] and Lewis G. Huey[3]

Received 8 August 2010; revised 1 March 2011; accepted 9 March 2011; published 1 June 2011.

[1] Airborne measurements of aerosol and cloud condensation nuclei (CCN) were conducted aboard the National Oceanic and Atmospheric Administration WP-3D platform during the 2006 Texas Air Quality Study/Gulf of Mexico Atmospheric Composition and Climate Study (TexAQS/GoMACCS). The measurements were conducted in regions influenced by industrial and urban sources. Observations show significant local variability of CCN activity (CCN/CN from 0.1 to 0.5 at s = 0.43%), while variability is less significant across regional scales (~100 km × 100 km; CCN/CN is ~0.1 at s = 0.43%). CCN activity can increase with increasing plume age and oxygenated organic fraction. CCN measurements are compared to predictions for a number of mixing state and composition assumptions. Mixing state assumptions that assumed internally mixed aerosol predict CCN concentrations well. Assuming organics are as hygroscopic as ammonium sulfate consistently overpredicted CCN concentrations. On average, the water-soluble organic carbon (WSOC) fraction is 60 ± 14% of the organic aerosol. We show that CCN closure can be significantly improved by incorporating knowledge of the WSOC fraction with a prescribed organic hygroscopicity parameter (κ = 0.16 or effective κ ~ 0.3). This implies that the hygroscopicity of organic mass is primarily a function of the WSOC fraction. The overall aerosol hygroscopicity parameter varies between 0.08 and 0.88. Furthermore, droplet activation kinetics are variable and 60% of particles are smaller than the size characteristic of rapid droplet growth.

Citation: Asa-Awuku, A., et al. (2011), Airborne cloud condensation nuclei measurements during the 2006 Texas Air Quality Study, *J. Geophys. Res.*, *116*, D11201, doi:10.1029/2010JD014874.

1. Introduction

[2] Atmospheric particles, by acting as cloud condensation nuclei (CCN), can indirectly influence climate through their impact on cloud radiative properties and the hydrological cycle [e.g., *Lohmann and Feichter*, 2005, and references therein]. The complexity and incomplete description of aerosol-cloud interactions in models result in large uncertainties in assessments of the anthropogenic indirect aerosol effect [e.g., *Haywood and Boucher*, 2000; *Ramanathan et al.*, 2001; *Lohmann and Feichter*, 2005; *Intergovernmental Panel on Climate Change (IPCC)*, 2007]. Much of this uncertainty in global climate models arises from the subgrid nature of cloud processes and the effect of poorly constrained parameters [e.g., *IPCC*, 2007], one of which is the CCN concentration. The prime factor controlling CCN concentration is the aerosol size distribution [*Twomey*, 1977; *Dusek et al.*, 2006]; however the variability of aerosol composition has also been shown to play a significant role in CCN activity [*Jimenez et al.*, 2009]. Predictions of CCN concentrations in climate models require simplifying assumptions, particularly in the description of chemical composition, and the resulting uncertainty in indirect forcing from their application need to be quantified [e.g., *Sotiropoulou et al.*, 2006].

[3] Each aerosol particle requires exposure to a "critical" level of water vapor supersaturation, s_c, before it can act as a CCN and activate into a cloud droplet. The s_c depends on the aerosol dry size and chemical composition, and is

[1]School of Chemical and Biomolecular Engineering, Georgia Institute of Technology, Atlanta, Georgia, USA.
[2]Department of Chemical and Environmental Engineering, Bourns College of Engineering-Center for Environmental Research and Technology, University of California, Riverside, California, USA.
[3]School of Earth and Atmospheric Sciences, Georgia Institute of Technology, Atlanta, Georgia, USA.
[4]Chemical Sciences Division, Earth System Research Laboratory, National Oceanic and Atmospheric Administration, Boulder, Colorado, USA.
[5]Cooperative Institute for Research in Environmental Sciences, University of Colorado at Boulder, Boulder, Colorado, USA.
[6]Department of Chemistry and Biochemistry and Department of Atmospheric and Oceanic Sciences, University of Colorado at Boulder, Boulder, Colorado, USA.

0148-0227/11/2010JD014874

computed from considering solute and curvature effects on the equilibrium water vapor pressure [*Köhler*, 1936]. "Köhler theory" remains to date the basis for linking CCN activity with aerosol thermophysical properties, and is used in all physically based models of the indirect effect to predict CCN number concentrations from knowledge of the aerosol size distribution, chemical composition and dynamical forcing. The simpler forms of Köhler theory involve aerosol composed of an "insoluble" and completely soluble fraction, and have been successfully applied to water-soluble inorganic and low molecular-weight organic aerosol. Simple forms of the theory may be subject to uncertainty when partially soluble compounds are present or when the aerosol is a complex mixture of inorganic and organic compounds. A comprehensive theory can become quite complex, as the presence of multiple phases and all the interactions of organics and inorganics with water must be accounted for, and requires the knowledge of poorly constrained parameters. This is especially true if the aerosol contains substantial amounts of ambient water-soluble organic carbon (WSOC), which can contribute solute [*Shulman et al.*, 1996], act as a surfactant that depresses droplet surface tension [*Facchini et al.*, 1999; *Decesari et al.*, 2003; *Asa-Awuku et al.*, 2008] and, potentially affect the condensation rate of water onto growing droplets [e.g., *Feingold and Chuang*, 2002; *Chuang*, 2003; *Nenes et al.*, 2002b; *Asa-Awuku et al.*, 2009].

[4] "CCN closure," or comparison of predictions with observations of ambient CCN concentrations, has been the focus of numerous studies and is the ultimate test of Köhler theory [e.g., *Liu et al.*, 1996; *Covert et al.*, 1998; *Ji et al.*, 1998; *Snider and Brenguier*, 2000; *Cantrell et al.*, 2001; *Dusek et al.*, 2003; *Roberts et al.*, 2003; *VanReken et al.*, 2003; *Rissler et al.*, 2004; *Broekhuizen et al.*, 2006; *Gasparini et al.*, 2006; *Rissman et al.*, 2006; *Roberts et al.*, 2006; *Yum et al.*, 2006; *Chang et al.*, 2007; *Medina et al.*, 2007; *Stroud et al.*, 2007; *Ervens et al.*, 2007; *Vestin et al.*, 2007; *Sorooshian et al.*, 2008; *Cubison et al.*, 2008; *Quinn et al.*, 2008; *Lance et al.*, 2009; *Shinozuka et al.*, 2009; *Bougiatioti et al.*, 2009; *Gunthe et al.*, 2009; *Hegg et al.*, 2009; *Murphy et al.*, 2009; *Wang et al.*, 2010; *Rose et al.*, 2010]. Most closure studies are based on ground site measurements, although the recent advent of CCN and aerosol instrumentation with very fast sampling frequency (~1 Hz) will ensure that airborne process-oriented studies will appear more frequently in the literature. Apart from establishing the applicability of Köhler theory, closure studies can be used to quantify the CCN prediction uncertainty associated with simplifying assumptions commonly used in models regarding aerosol mixing state, variation of composition with size and affinity of carbonaceous material with water. For example, *Broekhuizen et al.* [2006] and *Stroud et al.* [2007] found that omitting size-resolved composition and treating the organics as insoluble leads to a 30–50% CCN prediction bias. *Ervens et al.* [2007] found that neglecting the hygroscopicity of the organic fraction (i.e., treating the organic as insoluble) had little effect on CCN closure for aerosol sampled at Chebogue Point during the ICARTT 2004 campaign. Based on CCN measurements obtained at Thompson Farm during ICARTT 2004, *Medina et al.* [2007] found that usage of size-averaged chemical composition can lead to significant CCN concentration overpredictions. *Sotiropoulou et al.* [2006, 2007] further processed the *Medina et al.* [2007] data set and propagated the CCN prediction error in a global model simulation of the indirect effect; they concluded that simplified implementations of Köhler theory could introduce a 30% uncertainty in global annual average CCN concentrations that results in a 20–40% uncertainty in the model-derived indirect forcing of -1 W m^{-2}. *Cubison et al.* [2008] found that omission of size-resolved composition and aerosol mixing state information in a polluted urban site (Riverside, California) may bias calculated CCN concentrations by a factor of 2. *Quinn et al.* [2008] found that changes in composition can account for a 40% difference in CCN activity of boundary layer marine aerosol in the Gulf of Mexico, Texas. In the same region, *Lance et al.* [2009] found that different assumptions concerning the internally mixed chemical composition result in average CCN overprediction ranging from 3% to 36%; it is hypothesized that the externally mixed fraction of the aerosol contributes much of the CCN closure scatter, while the internally mixed fraction largely controls the overprediction bias. *Bougiatioti et al.* [2009] found particles in the Eastern Mediterranean were significantly aged, mostly activating at ~0.6% supersaturation; organic solubility assumptions improved CCN closure. *Gunthe et al.* [2009] observed CCN properties in pristine tropical rain forest air in Amazonia and observe good agreement (to within ~20% deviation) by including both hygroscopicity and organic fraction data into their predictions which were consistent with biogenic SOA. *Rose et al.* [2010] measured CCN in polluted air and biomass burning smoke at a rural site ~60 km northwest of the megacity Guangzhou in southeastern China. The inferred hygroscopicity parameters ranged from 0.1 to 0.5 for their measurements. *Rose et al.* [2010] then used a constant average hygroscopicity parameter equal to 0.3 and variable size distributions for closure studies and deviations were on average less than 20%. *Wang et al.* [2010] at a ground site in Mexico City, Mexico, observed significant changes in CCN activity and aerosol mixing during the daytime. For their closure, *Wang et al.* [2010] showed during daytime, and for a few tens of kilometers away from anthropogenic sources, that CCN concentrations may be derived with sufficient accuracy by assuming an internal mixture and using bulk chemical composition.

[5] Another important and poorly constrained aspect of cloud droplet formation is the kinetics of CCN activation. In cloud physics studies, droplet growth is largely controlled by the water vapor mass transfer to the condensed phase. It has been hypothesized that organics could dissolve slowly and form films that retard the uptake of water vapor molecules the droplet surface [e.g., *Feingold and Chuang*, 2002; *Chuang*, 2003]; this could then reduce the rate of condensation, with important impacts on the droplet number that forms in ambient clouds [*Nenes et al.*, 2002a; *Feingold and Chuang*, 2002; *Lance et al.*, 2004].

[6] Delays in the activation kinetics are often expressed as changes in the effective water vapor uptake coefficient, α (defined as the fraction of water molecules that are incorporated into a droplet upon collision with it). Values of $\alpha \sim 0.042$ were used in earlier cloud modeling studies for inorganic aerosol [*Lance et al.*, 2004; *McFiggans et al.*, 2006] reports a range of α from 0.04 to 1. *Conant et al.* [2004], *Meskhidze et al.* [2005], and *Fountoukis et al.* [2007] conducted aerosol-cloud droplet closure using in situ observa-

Table 1. Research Flights During TexAQS II 2006

Flight	Date	Flight and Source Characteristics	Wind Direction
1	20 Sep	Beaumont Port Arthur, Houston, Urban, Parrish Power Plant, Isolated refineries	Easterlies
2	21 Sep	Texas City, Houston Urban Plume	Southerlies
3	25 Sep	Dallas, Houston Urban Plume,Big Brown and Limestone power plants emission characterization and chemical processing	Northerlies
4	26 Sep	Houston Urban Plume and Industrial Sources, Parrish power plant, Beaumont, Port Arthur, Lake Charles emission characterization and chemical processing	Northerlies
5	27 Sep	Houston Urban Plume and Industrial Sources, Parrish Power Plant	South Westerlies
6	29 Sep	Houston Urban and Industrial, Parrish power plant emission characterization, nocturnal chemical processing.	Light winds, switching between Easterlies and Southerlies
7	5 Oct	Houston Urban and Industrial, Parrish power plant plume, Chemical Processing and Transport	Light winds, North Easterlies
8	6 Oct	Houston Urban and Industrial, Parrish Power Plant Plume, Chemical Processing and Transport	North Easterlies
9	8 Oct	Houston Urban and Industrial Parrish Power Plant Plume Emission Characterization, Chemical Processing and Nocturnal Transport	Light Easterlies
10	10 Oct	Oklaunion Power Plant (near Vernon, Texas) emission characterization, nocturnal chemical processing.	Northerlies to North Westerlies

tions of cumuliform and stratiform clouds formed in polluted and clean air masses; both studies achieved closure for α between 0.03 and 1.0, with optimum estimates (i.e., both average error and standard deviation within experimental uncertainty) between 0.03 and 0.06. *Stroud et al.* [2007], using a static diffusion chamber combined with a model of the instrument estimated $\alpha = 0.07$ for ambient anthropogenically influenced biogenic CCN sampled during the CELTIC experiment. *Ruehl et al.* [2008] observed a wide range of growth kinetics for ambient aerosol sampled in sites across the northern Unites States, and *Ruehl et al.* [2009] observed evidence of distinct activation kinetics associated with aerosol from outside the marine boundary layer. Recently, *Shantz et al.* [2010] also observed reduced droplet growth of aerosol particles containing anthropogenic organic components in Egbert, Ontario, Canada.

[7] This study further expands upon published work and uses airborne measurements of CCN concentration, aerosol size distribution and chemical composition measured in Houston, Texas during the Texas Air Quality Study 2006 (TexAQS II 2006) to determine (1) the error in predicted CCN concentrations associated with simplifying assumptions of the chemical composition and mixing state of CCN, (2) the effects of ageing and mixing processes on CCN activity, and (3) the impact of organics on CCN activity, hygroscopicity and the condensational growth of activated droplets. This study complements the work of *Quinn et al.* [2008] and *Lance et al.* [2009], who during the same campaign sampled CCN aboard the NOAA ship *Ronald H. Brown* and the Center for Interdisciplinary Remotely-Piloted Aircraft Studies (CIRPAS) Twin Otter aircraft, respectively.

2. Observational Data Set and Instrumentation

2.1. Study Location and Flight Trajectories

[8] The Texas Air Quality Study (TexAQS) and Gulf of Mexico Climate Change Study (GoMACCS) were conducted using several platforms (e.g., ground-based, airborne, ship, and satellite overpasses) in August through October of 2006. The goals of the combined studies were to observe the spatiotemporal distribution of atmospheric constituents, understand the transport of pollutants in the Eastern Texas and Northern Gulf of Mexico region, and, characterize their impacts on air quality and regional climate [*Parrish et al.*, 2009]. The data in this study were obtained aboard the National Oceanic and Atmospheric Administration (NOAA) WP-3D aircraft from September to October 2006. Table 1 reports the 10 research flights for which CCN data were collected. Ambient aerosol was sampled by the WP-3D using a low turbulence inlet (LTI) [*Huebert et al.*, 2004; *Wilson et al.*, 2004], during which a laminar deceleration of the airstream ensured minimal particle losses for submicron aerosol (hence CCN) [*Wilson et al.*, 2004; *Brock et al.*, 2008].

[9] The studied region is characterized by strong and diverse urban and industrial pollution sources. The Houston ship channel hosts many petrochemical refineries and there are several large coal-fired power plants in the east Texas region (e.g., Parrish, Big Brown, Limestone). The fine particulate mass in urban environments tends to be dominated by sulfates and organics [e.g., *Zappoli et al.*, 1999]; this was found to be true for Houston as well.

2.2. Aerosol Size Distribution Measurements

[10] A white-light Optical Particle Counter (OPC), an UltraHigh Sensitivity Aerosol Size spectrometer (UHSAS) and a Nucleation Mode Aerosol Size Spectrometer (NMASS) were used to measure the aerosol dry size distribution from 0.003 to 8.3 μm diameter at a 1 Hz frequency. Other than UHSAS data, the particle size distribution measurement and analysis techniques are similar to that used aboard the WP-3D during the 2004 New England Air Quality Study (NEAQS) [*Brock et al.*, 2008]. Ultrafine particles (diameter <0.1 μm) were measured using five condensation particle counters (CPCs), set to measure particle concentrations down to 0.004, 0.008, 0.015, 0.030, and 0.055 μm diameter with a 50% detection efficiency at these sizes. Size distributions were derived from the observed

concentrations in the five size classes, coupled with a nonlinear inversion algorithm [*Markowski*, 1987]. A complete description of the instrument methodology and data analysis is provided by *Brock et al.* [2008].

2.3. CCN Measurements

[11] A Droplet Measurement Technologies Continuous-Flow Streamwise Thermal Gradient Chamber (CFSTGC) [*Roberts and Nenes*, 2006; *Lance et al.*, 2006] was used to measure CCN concentrations. A constant temperature gradient is applied across the internal wetted wall of the instrument flow chamber; the difference in the radial diffusive flux of water vapor and heat generates a supersaturation, s, which is maximum at the centerline [*Roberts and Nenes*, 2006; *Lance et al.*, 2006]. Aerosol is introduced along the centerline of the flow chamber and exposed to s. The fraction whose "critical" supersaturation, s_c, is less then s activate into cloud droplets and an optical particle counter at the exit of the flow chamber then detects the concentration and size distribution of activated droplets. s in the CFSTGC is a function of pressure, flow rate and temperature gradient in the flow chamber. The s is calibrated for a given set of chamber conditions using the procedure of *Asa-Awuku et al.* [2009]. This includes determining the minimum diameter, d, of calibration $(NH_4)_2SO_4$ aerosol (generated by atomization of an aqueous $(NH_4)_2SO_4$ solution with a Collison-type atomizer, which is subsequently dried and classified with a differential mobility analyzer) that activates in the instrument; d is then related to s by applying Köhler theory using an effective van't Hoff factor computed using the ion interaction approach of *Pitzer and Mayorga* [1973] with parameters obtained from *Clegg and Brimblecombe* [1988]. The effective van't Hoff factor was computed at the molality corresponding to the critical diameter of the CCN. This procedure is repeated over a wide range of temperature and pressures. Bilinear interpolation of the calibrations to the pressure and temperature conditions occurring in flight is used to determine the instrument s during the measurements.

[12] The CFSTGC sampled aerosol from the LTI at a flow rate of 1000 cm^3 min^{-1}, over a supersaturation range of 0.1% to 0.6%. The instrument was operated in a "temperature stepping mode" during which flow and temperature conditions are maintained constant during the measurement interval. The instrument pressure varied with altitude and was approximately equal to the ambient pressure. During the first two flights, the temperature difference across the column, ΔT, was set to 4.2 ± 0.1°K, corresponding to a s equal to 0.3 ± 0.05%. In the remaining research flights, ΔT was cycled over 3 min intervals between 5.2 and 7°K, varying s from 0.42 ± 0.05% to 0.74 ± 0.05%. The reported variability accounts for the measured fluctuations in temperature gradient and instrument pressure. Data collected during shifts in instrument temperature (e.g., due to cabin temperature, pressure, or supersaturation changes) and pressure (during altitude changes) are filtered, as described in section 3.

2.4. Chemical Composition Measurements

[13] An Aerodyne aerosol mass spectrometer (AMS) measured size-resolved mass distributions and total mass loadings of nonrefractory chemical species in submicron aerosol. During TexAQS, a compact time-of-flight AMS (C-ToF-AMS) with a pressure controlled inlet was used [*DeCarlo et al.*, 2006; *Drewnick et al.*, 2005; *Canagaratna et al.*, 2007; *Bahreini et al.*, 2008]. Within the instrument, the sampled particles are focused in to a beam and impact on a vaporizer located within the electron ionization source region of a mass spectrometer. When operated in the "particle time of flight" (PToF) mode, mass distributions of nonrefractory species are obtained by interrupting the particle beam with a chopper and measuring the time particles take to traverse the vacuum chamber before detection. When operated in the "mass spectrum" mode, spectra with a mass-to-charge ratio (m/z) of 1 to 220 are collected from multiple particles with good time resolution (~10 s) at the expense of size dependence. From characteristic mass spectral ion signals, quantitative concentrations for sulfate, nitrate, ammonium, organic mass and inferred oxygenated content are obtained [*Jimenez et al.*, 2003; *Allan et al.*, 2003, 2004; *Bahreini et al.*, 2003; *Schneider et al.*, 2004].

[14] Analysis of specific m/z signals provides information about the degree to which the organic species are oxidized. For example, the organic signal at m/z 44 (mostly CO_2^+) is strongly correlated with the amount of oxygenated organic aerosol (OOA), a surrogate for SOA [*Zhang et al.*, 2005; *Aiken et al.*, 2009]. The organic ion signal from $C_4H_7^+$, which can be estimated as the total signal at m/z 57 minus a correction of 5% of the m/z 44 (to account for the contribution of $C_3H_5O^+$, an OOA fragment to m/z 57) is strongly correlated with hydrocarbon-like organic aerosol (HOA), a surrogate for primary combustion OA in urban areas [*Zhang et al.*, 2005; *Aiken et al.*, 2009].

[15] A Particle-into-Liquid sampler (PILS) captured ambient particles and dissolved them into ultrapurified water [*Orsini et al.*, 2003]. The stream containing soluble materials was then filtered and measured with a Total Organic Carbon (TOC) Analyzer to quantify the WSOC concentration. Additional information about the WSOC measurement, analysis, and calibration is provided by *Orsini et al.* [2003] and *Sullivan and Weber* [2006].

3. Data Analysis and CCN Prediction

[16] CCN closure calculations were carried out using 30 second averages of CCN, aerosol size distribution and chemical composition measurements. Prior to the averaging, data from the CCN counter were filtered to remove temperature transients (during supersaturation changes) and pressure transients (during rapid altitude changes). At a given time, t, data is averaged over a 30 second window centered around t; averages for which pressure fluctuates more than ±0.5% from the mean, and, temperatures more than ±0.05°K about its average are removed from the analysis.

3.1. Predicting CCN Concentrations

[17] The measured aerosol size distributions and chemical compositions were used to predict CCN concentrations with Köhler theory. CCN activity is characterized by the critical dry diameter, d_c, defined as the minimum particle size (of a given composition) that activates at the instrument supersaturation, s; particles are then classified as CCN if their physical diameter is larger than d_c (this is equivalent to

stating that particles have a s_c less than the instrument supersaturation, s). The s_c was calculated by applying Köhler theory, assuming that the aerosol is composed of a mixture of soluble and insoluble fractions [*Medina et al.*, 2007; *Seinfeld and Pandis*, 2006],

$$d_c = \left(s^2 \frac{27}{256} \left(\frac{\rho_w RT}{M_w \sigma} \right)^3 \left(\frac{M_w}{\rho_w} \sum_s \frac{\rho_s}{M_s} \nu_s \varepsilon_s \right) \right)^{-1/3}, \quad (1)$$

where R is the universal gas constant, T is the average temperature across the CFSTGC flow column, σ is the droplet surface tension at the point of activation (calculated at T), M_s is the molar mass of each solute, M_w is the molar mass of water, ρ_w is the density of water, and ν_s is the effective van't Hoff factor of the solute. ε_s is the volume fraction of each solute, computed assuming volume additivity as

$$\varepsilon_s = \frac{\frac{m_s}{\rho_s}}{\sum_j \frac{m_j}{\rho_j}}, \quad (2)$$

where m_j and ρ_j are the mass fraction and density, respectively, of aerosol component "j" (which includes all soluble and insoluble compounds).

[18] The density of the organic fraction was assumed to be 1270 kg m^{-3} [*Cross et al.*, 2007]. Ammonium and sulfate dominate the inorganic aerosol dry mass, indicative of ammonium sulfate salts, the speciation of which depends on the molar ratio of ammonium to sulfate ions, R_{SO4} [*Nenes et al.*, 1998], as follows: (1) $R_{SO4} < 1$, the soluble fraction is a mixture of sulfuric acid (M_s = 0.098 kg mol^{-1}, ρ_s = 1841 kg m^{-3}) and ammonium bisulfate (M_s = 0.115 kg mol^{-1}, ρ_s = 1780 kg m^{-3}), as determined from the mass balance, (2) $1 < R_{SO4} < 2$, the soluble fraction is a mixture of ammonium bisulfate and ammonium sulfate (M_s = 0.132 kg mol^{-1}, ρ_s = 1760 kg m^{-3}), as determined from the mass balance, and (3) $R_{SO4} > 2$, the soluble fraction is composed of pure ammonium sulfate. R_{SO4} was almost never below unity (i.e., free H_2SO_4 was not present in the aerosol), as is typical for measurements over continental boundary layers where sources of ammonia are relatively strong [*Zhang et al.*, 2007; *Salcedo et al.*, 2006]. The relative humidity of the sampled aerosol was less than 10%. Therefore, residual water can be assumed to be negligible in the dry aerosol sampled onboard the aircraft [*Murphy et al.*, 2009].

[19] Consistent with the level of acidity in the particles, nitrate salts constitute a minor fraction of the soluble ions (<5% of the total), but are included in the CCN activity calculations. The effective van't Hoff factor applied for each of the salts during calculation of d_c was computed using the parameterized Pitzer water activity correlations [*Pitzer and Mayorga*, 1973; *Clegg and Brimblecombe*, 1988] at the molality corresponding to the critical diameter of the CCN.

[20] Nonrefractory material, such as black carbon (also measured aboard the aircraft by a Single-Particle Soot Photometer [*Schwarz et al.*, 2006]), did not contribute significant particulate mass (<2% mass fraction) and was therefore not considered in the different CCN schemes. This is consistent with *Lance et al.* [2009], who found that BC is a minor aerosol constituent, except for flights in the ship channel where neglecting its mixing state could lead to large CCN overpredictions. Since transmission of particles in the AMS inlet drops below 50% for particles with physical diameter smaller than 50 nm and larger than 640 nm, the measured aerosol composition outside this range is limited [*Bahreini et al.*, 2009]. The composition of the smallest particles detected by the AMS was hence uniformly applied to aerosol smaller than 50 nm (physical diameter). On average, this assumption impacts <~15% of the total particles that may become CCN.

[21] Six compositional schemes were employed in this study for CCN closure calculations:

[22] 1. In the inorganic (INORG) scheme, the aerosol volume is composed of an inorganic solute mixture consistent with the inorganic portion of the AMS bulk composition data. This scheme represents an upper limit of CCN activity, as the organic fraction is implicitly assumed to have the same hygroscopic properties as the inorganic fraction.

[23] 2. In the bulk composition externally mixed (BK-EX) scheme, the aerosol is an external mixture of two populations (i.e., soluble, "inorganic-only" particles and insoluble, "organic-only" particles), the relative amounts of which are determined from the bulk AMS composition measurements. The "organic-only" particles are assumed nonhygroscopic and do not contribute CCN; the "inorganic-only" particles are composed of a mixture of salts, as determined by the AMS compositional data. The composition is assumed uniform across the entire size distribution.

[24] 3. In the bulk composition internally mixed (BK-INT) scheme, aerosol is an internal mixture of insoluble organic and inorganic salts, as determined by the AMS bulk compositional data. The composition is uniform across the size distribution.

[25] 4. In the size-resolved composition externally mixed (SR-EX) scheme, aerosol is an external mixture of "organic-only" and "inorganic-only" particles. Again, the "organic-only" particles are assumed nonhygroscopic. In contrast to the BK-EX scheme, size-resolved composition data from the AMS is applied, meaning that the relative concentration of each population varied with size.

[26] 5. In the size-resolved composition internally mixed (SR-INT) scheme, aerosol is an internal mixture of organic and inorganic salts, as determined by the size-resolved AMS bulk compositional data.

[27] 6. In the bulk composition internally mixed soluble fraction (BK-INT-SOL) scheme, similar to the BK-INT scheme, except now organics are hygroscopic. The aerosol is an internal mixture of organic and ammoniated sulfate salts, as determined by the AMS bulk compositional data. The composition is assumed to be uniform across the entire size distribution. A fraction of the organic mass, equal to the ratio of PILS WSOC to AMS organic mass, is assumed soluble with a molar volume of $\frac{M}{\rho}$ = 1.48 × 10^{-4} m^3 mol^{-1}, effective van't Hoff factor of $\nu = 1$, and 10% surface tension depression with respect to pure water. In this study, the WSOC/OC is converted to WSOC/OM by a factor of 1.5 [*Wolff et al.*, 1991; *Seinfeld and Pandis*, 2006]. For aerosol containing mostly OOA, this value may be higher (~1.8 to 2.1 [*Turpin and Lim*, 2001; *Aiken et al.*, 2008]). The lower factor limit is used to account for less oxygenated organic aerosol found near emission sources. For significantly oxygenated organics a factor of 1.5 will contribute up to −20% error in our soluble fraction estimates. The WSOC

properties represent average values for WSOC obtained from biomass burning aerosol, cycloheptene, methylcycloheptene, terpinolene, monoterpene and β-caryophyllene SOA [*Asa-Awuku et al.*, 2010, 2008; *Engelhart et al.*, 2008; *Asa-Awuku et al.*, 2009] and is consistent with the CCN properties of SOA from Mexico City aerosol [*Padró et al.*, 2010]. Analysis of the inferred hygroscopicity parameter (section 4.5) confirms that the assumed WSOC molar volume used here is a reasonable choice.

[28] Only bulk WSOC measurements were available, hence it was not possible to relax the bulk composition assumption by employing a size-resolved, internally mixed, soluble (SR-INT-SOL) scheme. In schemes other than BK-INT-SOL, organics do not contribute solute nor affect surface tension. σ for pure water in all schemes is computed at the average column temperature of the CFSTGC, which ranges between 30 and 45°C. In the closure studies of *Chang et al.* [2007] and *Lance et al.* [2009], some contribution of organic solute and/or surface tension reduction was necessary to improve CCN predictions and minimize bias; BK-INT-SOL goes beyond these studies in that measured WSOC/OC is used as a predictor of hygroscopicity for the organic fraction.

3.2. Evaluating Predictions Against Observations

[29] CCN predictions are compared to observed concentrations for the schemes described above. Results were summarized in terms of the slope, S, and variance, R^2, between predicted and measured data (assuming a linear fit between the two, with an intercept of zero). Deviation greater than 10% from $S = 1$ was assumed to show disagreement in closure; $S > 1$ (CCN overprediction) and $S < 1$ (underprediction) are potentially due to an overestimation or underestimation of soluble and surface active materials, respectively. R^2 values close to unity suggest that errors from unaccounted compositional and size distribution variation, random errors and spatiotemporal fluctuations below the averaging time scale were small. We also represent closure in terms of the Normalized Mean Error (*NME*) and the Normalized Mean Bias (*NMB*),

$$NME = \frac{\sum_i^n |P_i - O_i|}{\sum_i^n O_i} \text{ and } NMB = \frac{\sum_i^n (P_i - O_i)}{\sum_i^n O_i} \quad (3)$$

where n is the number of measurements available; P_i and O_i are the predicted and observed CCN concentration, respectively. The *NME* indicates the degree of scatter between predictions and observations (small values suggest little scatter), and *NMB* reflects the degree of systematic errors (biases) between the predicted and measured values; a negative *NMB* is consistent with under prediction and vice versa. Other more comprehensive nonlinear error metrics could be used [*Cantrell*, 2008], but the differences between closure schemes are large enough so that the linear metrics presented here are sufficient for determining the better scheme. Large *NME* and *NMB* values derived from closure schemes are indicative of poorly assumed correlations and or parameterizations for CCN predictions. Hence the CCN prediction scheme that provides the best closure also has *NME* and *NMB* values close to zero.

3.3. Hygroscopicity Parameter κ Calculations

[30] The composition dependence of CCN activity may be expressed in terms of a single hygroscopicity parameter, κ [*Petters and Kreidenweis*, 2007],

$$\kappa = \frac{4A^3}{27 d_c^3 \ln^2 s}, \quad (4)$$

where $A = \frac{4\sigma_w M_w}{RT\rho_w}$; using the same symbols, equation (4) is derived from equation (1). As prescribed by *Petters and Kreidenweis* [2007], σ_w is the surface tension of water at average instrument temperature. If organics depress surface tension, to a value σ at the point of activation, application of equation (4) overestimates κ by a factor of $(1 - \frac{\sigma_w - \sigma}{\sigma_w})^{-3}$ [*Asa-Awuku et al.*, 2010]. For insoluble, wettable materials that do not impact water activity via adsorption [*Kumar et al.*, 2009], $\kappa = 0$, and increases with the addition of soluble compounds [*Petters and Kreidenweis*, 2007]. For $(NH_4)_2SO_4$, the most abundant inorganic compound observed during TexAQS, $\kappa = 0.6$. The κ value prescribing the values of WSOC from BK-INT-SOL = 0.16 with an effective $\kappa \sim 0.3$, assuming $\sigma = \sigma_{water}$. The effective κ value is within previously reported range of oxidized (hygroscopic) carbonaceous material [e.g., *Prenni et al.*, 2007; *Engelhart et al.*, 2008; *Jurányi et al.*, 2009; *Jimenez et al.*, 2009; *Asa-Awuku et al.*, 2010]. The κ values are presented in section 4.5 for the most robust CCN prediction scheme presented here that accounts for changing particle chemistry.

3.4. Droplet Growth and Kinetics Analysis

[31] When exposed to the same s profile (that exceeds their s_c) two CCN will activate and grow to cloud droplets of similar wet diameter, D_p, provided that their critical supersaturation and mass transfer coefficient of water vapor to the growing droplets is the same [*Nenes et al.*, 2001; *Roberts and Nenes*, 2006]. The CCN instrument measures the droplet size distribution after CCN activation, which can be used to explore the impact of aerosol composition on the droplet growth kinetics using the method of Threshold Droplet Growth Analysis (TDGA). TDGA compares the droplet sizes of activated ambient particles against a standard of rapid activation kinetics. The standard used in this study is the droplet size, D_r, of calibration $(NH_4)_2SO_4$ aerosol with $s_c = s$, being the minimum size droplet of rapidly activating CCN (e.g., an effective uptake coefficient, $\alpha \sim 0.1$–1). Ambient particles, if also growing fast, will yield droplet sizes equal or larger than D_r (because of the polydispersity of the ambient sample), and vice versa. As presented here, TDGA can only detect the presence of slowly activating CCN. Parameterizing delays in terms of α requires the use of a model [*Asa-Awuku et al.*, 2009; *Ruehl et al.*, 2008, 2009]. TDGA has been successfully applied in numerous studies [*Engelhart et al.*, 2008; *Moore et al.*, 2008; *Sorooshian et al.*, 2008; *Bougiatioti et al.*, 2009; *Murphy et al.*, 2009; *Lance et al.*, 2009; *Asa-Awuku et al.*, 2010, 2008, 2009], and shown that hygroscopic CCN tend to exhibit activation kinetics similar to $(NH_4)_2SO_4$; less hygroscopic CCN however can activate into droplets more slowly. A focus of this study is to explore the impact of composition on the activation kinetics of Houston aerosol. For large CCN concentrations in the instrument column

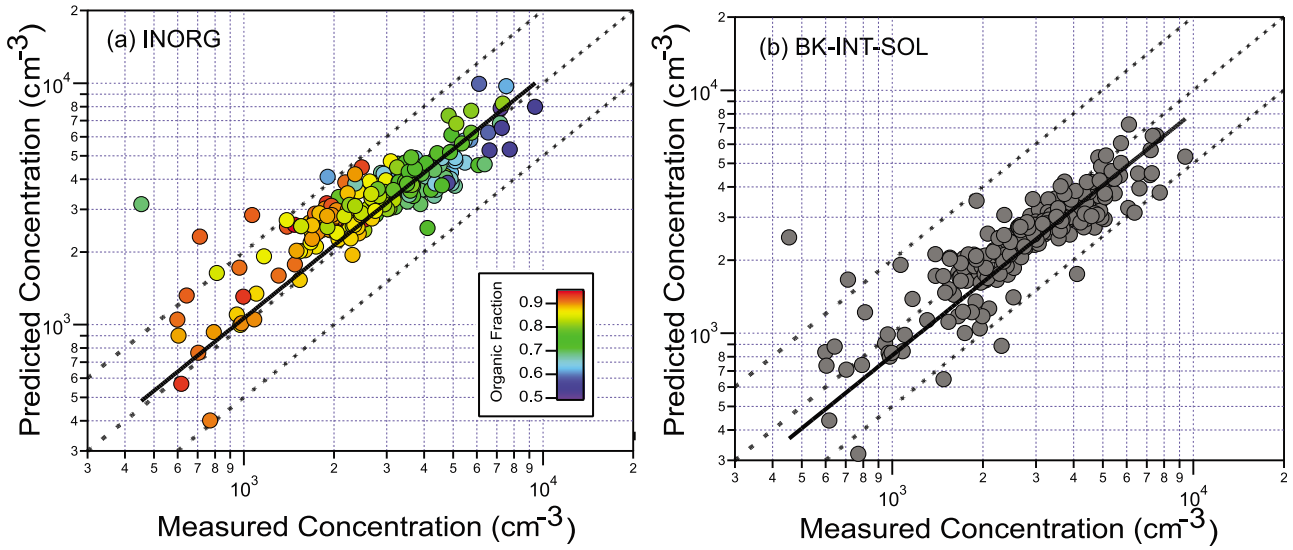

Figure 1. CCN closure plot for research flight 1 (20 September), for (a) INORG (where symbols are colored by organic volume fraction) and (b) BK-INT-SOL schemes. Dashed lines represent 1:1 perfect agreement (center) and 50% uncertainty.

(>5000 cm^{-3}) supersaturation depletion will occur in the CCN counter [*Lathem and Nenes*, 2011]; the droplet sizes have been corrected using the approach of *Lathem and Nenes* [2011]. Specifically, droplet growth sizes of CCN concentrations greater than 5000 cm^{-3} have been excluded from the TDGA analysis presented.

4. Results and Discussion

[32] Plumes within the Houston area quickly mix with background (regional) air. The "background" regional air is itself not uniform, but rather a mixture of aged air masses and plumes from various sources. Quantitatively following the ageing of aerosol thus becomes quite challenging; the exception is when the wind direction remains constant during a flight and a plume is transected at different locations downwind of its source. Assuming that the nature of emissions did not vary throughout the transects, "plume age" could be determined from the distance from the source "epicenter" (Ship Channel or Downtown centers) and the wind speed. A detailed explanation of the calculation and process used to distinguish plumes from background air with gas phase tracers is provided by *Bahreini et al.* [2009]. In sections 4.1–4.6, we discuss CCN behavior and predictions on regional and local scales for selected flights of interest during TexAQS/GOMACCS II 2006.

4.1. CCN Characteristics of Mixed Houston Plume Sources

[33] The research flight on 20 September was a 6.5 h mission that focused on the daytime urban atmospheric chemistry and the Houston area environment. The WP-3D departed in the eastward direction, transecting different plumes by traveling westward in a "zig-zag" flight pattern across industrial areas in the region. The aircraft transected two areas of concentrated plumes (CN concentrations >5 × 10^4 cm^{-3}); organics dominated the aerosol volume fraction (~0.7 to 0.9, auxiliary material Figure S4a).[1] The largest CN concentrations were observed near the ship channel and downtown areas. The aerosols were from different sources and had varied chemical compositions (auxiliary material Figure S1).

[34] Particle characteristics changed substantially during the flight (varying 1 order of magnitude in number concentration, ~10^4 to ~10^5 cm^{-3}, auxiliary material Figures S1 and S4a) as the aircraft sampled fresh emissions in downtown Houston and the ship channel, and more aged aerosol south and west of the urban center. Since most of the particles were <50 nm in diameter (smaller than the d_c required for their activation), only a small fraction were activated and measured as CCN. BK-INT-SOL and INORG schemes achieved the best closure for the 20 September flight (e.g., best closure S, $R^2 \sim 1$ and *NME* and *NMB* ~ 0; Table 2). For INORG, when CN counts increased, closure agreement shifted from strong overprediction at lower CCN concentrations (<3000 cm^{-3}) to a mostly unbiased scatter at higher concentrations (reflected in the relatively weak correlation between predictions and observations, $R^2 \simeq 0.65$; Table 2). Most of the INORG overprediction was observed in regions with relatively lower CN concentrations and high organic volume fraction (~0.9; Figure 1). Assuming that organics were insoluble (BK-INT and BK-EXT schemes) resulted in considerable underprediction of CCN concentrations and increased scatter (*NMB* and *NME* > 30%, Table 2), with BK-EXT giving the worst closure of all. All the above suggests that the aerosol tended to be internally mixed, with a partially soluble organic fraction that was less hygroscopic than sulfate salts, and with thermodynamic properties consistent with previous WSOC CCN studies. The INORG scheme gave much better closure within "polluted" (CN > 50 × 10^3 cm^{-3} on 20 September) than

[1] Auxiliary materials are available in the HTML. doi:10.1029/2010JD014874.

Table 2. Closure Analysis for TexAQS II 2006 Data Set[a]

Flight	Date	Average s	Error Metric	BK-INT-SOL	INORG	SR-INT	SR-EXT	BK-INT	BK-EXT
#1	20 Sep	0.30%	$S(R^2)$	0.81 (0.70)	1.06 (0.66)	NAMS	NAMS	0.68 (0.77)	0.25 (0.75)
			NME (NMB) (%)	19.3 (−15.5)	18.7 (11.6)	NAMS	NAMS	31.9 (−31.0)	76.2 (−76.1)
#2	21 Sep	0.30%	$S(R^2)$	0.93 (0.81)	1.13 (0.84)	NAMS	NAMS	0.77 (0.76)	0.35 (0.62)
			NME (NMB) (%)	17.9 (−2.1)	24.4 (15.3)	NAMS	NAMS	23.5 (−18.4)	60.6 (−60.0)
#3	25 Sep	0.43%	$S(R^2)$	0.66 (0.87)	0.73 (0.73)	0.45 (0.02)	0.28 (0.80)	0.44 (0.69)	0.35 (0.92)
			NME (NMB) (%)	26.9 (−21.2)	27.2 (−1.8)	34.5 (−28.8)	64.9 (−64.9)	40.1 (−39.8)	70.9 (−70.9)
		0.71%	$S(R^2)$	0.85 (0.74)	1.35 (0.88)	0.69 (0.19)	0.34 (0.18)	0.57 (0.19)	0.37 (0.85)
			NME (NMB) (%)	16.4 (−10.2)	38.6 (33.2)	31.4 (−22.9)	64.7 −3.2)	36.9 (−36.6)	65.0 (−65.0)
#4	26 Sep	0.44%	$S(R^2)$	NPILS	1.202 (0.63)	0.921 (0.64)	0.45 (0.62)	0.83 (0.65)	0.43 (0.63)
			NME (NMB) (%)	NPILS	32.6 (28.4)	22.1 (−1.4)	55.5 (−54.5)	23.5 (−11.9)	59.7 (−58.7)
		0.73%	$S(R^2)$	NPILS	1.16 (0.94)	0.81 (0.91)	0.43 (0.83)	0.84 (0.94)	0.48 (0.88)
			NME (NMB) (%)	NPILS	18.8 (17.5)	16.8 (−15.7)	60.5 (−60.5)	14.8 (−14.5)	59.0 (−59.0)
#5	27 Sep	0.44%	$S(R^2)$	0.96 (0.78)	1.108 (0.78)	0.89 (0.76)	0.49 (0.73)	0.80 (0.76)	0.41 (0.68)
			NME (NMB) (%)	13.6 (−3.0)	−14.9 (−9.8)	15.7 (−6.9)	53.7 (−52.3)	21.5 (−16.7)	62.9 (−61.7)
		0.74%	$S(R^2)$	0.96 (0.94)	1.05 (0.93)	0.88 (0.90)	0.45 (0.80)	0.86 (0.93)	0.39 (0.86)
			NME (NMB) (%)	9.4 (−5.8)	10.4 (−5.6)	15.4 (−12.8)	56.3 (−56.3)	16.2 (−14.9)	63.7 (−63.7)
#6	29 Sep	0.44%	$S(R^2)$	1.03 (0.93)	1.20 (0.88)	0.99 (0.88)	0.48 (0.76)	0.88 (0.90)	0.44 (0.60)
			NME (NMB) (%)	7.5 (2.7)	16.7 (15.2)	12.5 (−3.1)	52.4 (−52.4)	12.5 (-10.7)	54.3 (−54.3)
		0.74%	$S(R^2)$	1.02 (0.97)	1.15 (0.93)	0.90 (0.92)	0.44 (0.85)	0.89 (0.98)	0.41 (0.79)
			NME (NMB) (%)	7.2 (0.9)	14.0 (10.6)	13.3 (−10.9)	56.7 (−56.7)	11.0 (−10.5)	57.4 (−57.4)
#7	5 Oct	0.43%	$S(R^2)$	0.95 (0.90)	1.00 (0.89)	0.83 (0.83)	0.44 (0.87)	0.84 (0.86)	0.49 (0.89)
			NME (NMB) (%)	11.5 (−2.8)	12.4 (2.8)	16.9 (−12.6)	56.4 (−56.4)	15.7 (−11.9)	52.4 (−52.4)
		0.72%	$S(R^2)$	1.00 (0.88)	1.08 (0.82)	0.82 (0.76)	0.40 (0.62)	0.89 (0.90)	0.49 (0.80)
			NME (NMB) (%)	10.0 (0.2)	13.9 (7.7)	17.4 (−15.7)	59.6 (−59.6)	12.6 (−10.8)	51.7 (−51.7)
#8	6 Oct	0.43%	$S(R^2)$	1.01 (0.92)	1.17 (0.90)	NAMS	NAMS	0.85 (0.92)	0.42 (0.80)
			NME (NMB) (%)	11.5 (−0.5)	18.5 (14.6)	NAMS	NAMS	17.6 (−14.5)	61.3 (−61.3)
		0.71%	$S(R^2)$	0.97 (0.95)	1.12 (0.87)	NAMS	NAMS	0.85 (0.97)	0.33 (0.79)
			NME (NMB) (%)	7.2 (−3.3)	13.5 (10.4)	NAMS	NAMS	14.3 (−14.3)	66.4 (−66.4)
#9	8 Oct	0.43%	$S(R^2)$	0.94 (0.42)	1.02 (0.47)	NAMS	NAMS	0.85 (0.35)	0.38 (0.46)
			NME (NMB) (%)	12.4 (−3.5)	10.4 (4.3)	NAMS	NAMS	19.0 (−13.4)	61.5 (−61.5)
		0.73%	$S(R^2)$	0.90 (0.85)	0.95 (0.79)	NAMS	NAMS	0.85 (0.84)	0.35 (0.79)
			NME (NMB) (%)	10.1 (−8.8)	7.2 (−3.9)	NAMS	NAMS	15.4 (−14.8)	65.4(−65.4)
#10	10 Oct	0.42%	$S(R^2)$	1.06 (0.15)	1.15 (0.05)	NAMS	NAMS	0.96 (0.25)	0.43 (−0.81)
			NME (NMB) (%)	13.1 (10.3)	19.0 (18.3)	NAMS	NAMS	11.4 (−1.2)	55.0 (−54.4)
		0.65%	$S(R^2)$	1.04 (0.63)	1.08 (0.56)	NAMS	NAMS	0.95 (0.79)	0.43 (−0.54)
			NME (NMB) (%)	8.3 (4.9)	10.4 (9.5)	NAMS	NAMS	7.9 (−4.7)	55.8 (−55.8)
All Flights		all s	S	0.94 ± 0.10	1.09 ± 0.13	0.82 ± 0.15	0.42 ± 0.07	0.81 ± 0.13	0.40 ± 0.06
			NMB (%)	−3.6 ± 7.7	11.6 ± 9.3	−13.1 ± 8.4	−57.7 ± 4.3	−16.1 ± 10.0	−60.9 ± 6.4

[a] S is the slope of the fit of the data, and R^2 is the correlation coefficient. S and R^2 values >0.9 indicate good closure and agreement. The normal mean error, NME, indicates the degree of scatter, and normal mean bias, NMB, reflects the degree of systematic errors from perfect closure agreement. NAMS, no size-resolved AMS measurements applied; NPILS, no PILS-WSOC measurements available.

"nonpolluted" regions (Figure 1); this indicates that sulfate aerosol is the largest contributor to CCN concentrations in the most polluted areas sampled during TexAQS. Although size-resolved composition measurements were not available to confirm this, the rapid changes in gas-phase concentrations of SO_2 in these regions are consistent with this view (auxiliary material Figure S5a). Nevertheless, organics are expected to be present in CCN-relevant sizes; their lower hygroscopicity (compared to inorganic sulfate and nitrate) may be partially compensated by surface tension depression [*Asa-Awuku et al.*, 2008, 2010; *Padró et al.*, 2007]. Hence results from 20 September also suggest that in the absence of compositional information, one can assume properties of $(NH_4)_2SO_4$ when computing CCN near strong SO_2 pollution sources.

[35] The research flight on 21 September 2006 characterized urban and ship channel particle sources and their evolution while being advected northward (auxiliary material Figure S2). The flight on 21 September was of particular interest because a shift in CCN behavior was observed in different locations within the metropolitan area, downwind of the urban and industrial centers after 1900 UTC (auxiliary material Figure S4b). Anthropogenic particles are a convolution of plumes from several aged sources hence separating the contribution from individual plumes is very challenging. Therefore, analysis for this flight was limited to changes in CCN with latitude, north of downtown (Figure 2). (A plume evolution analysis for distinct sources is found in section 4.3). Near downtown Houston, CCN concentrations remained fairly insensitive to fluctuations in total CN (auxiliary material Figure S4b, before 1830 UTC), which are mostly from particles too small to activate in the range of s considered. The activated ratio (CCN/CN), size and organic fraction increased as particulate concentrations decreased (Figure 2 and auxiliary material Figure S4b). This trend is consistent with changes in particle composition, as it is accompanied by a slight increase in the ratio of oxygenated to nonoxygenated organic AMS markers (m/z 44/57; Figure 2). As on 20 September, despite changes in aerosol composition and flight location, the average activated droplet size in the CFSTGC throughout the flight (2.05 ± 0.45 μm) was similar to droplet sizes from activation of calibration $(NH_4)_2SO_4$ (2.06 ± 0.2 μm, auxiliary material Figure S5b). The droplet size distribution from activation of ambient CCN in the CFSTGC are much broader than

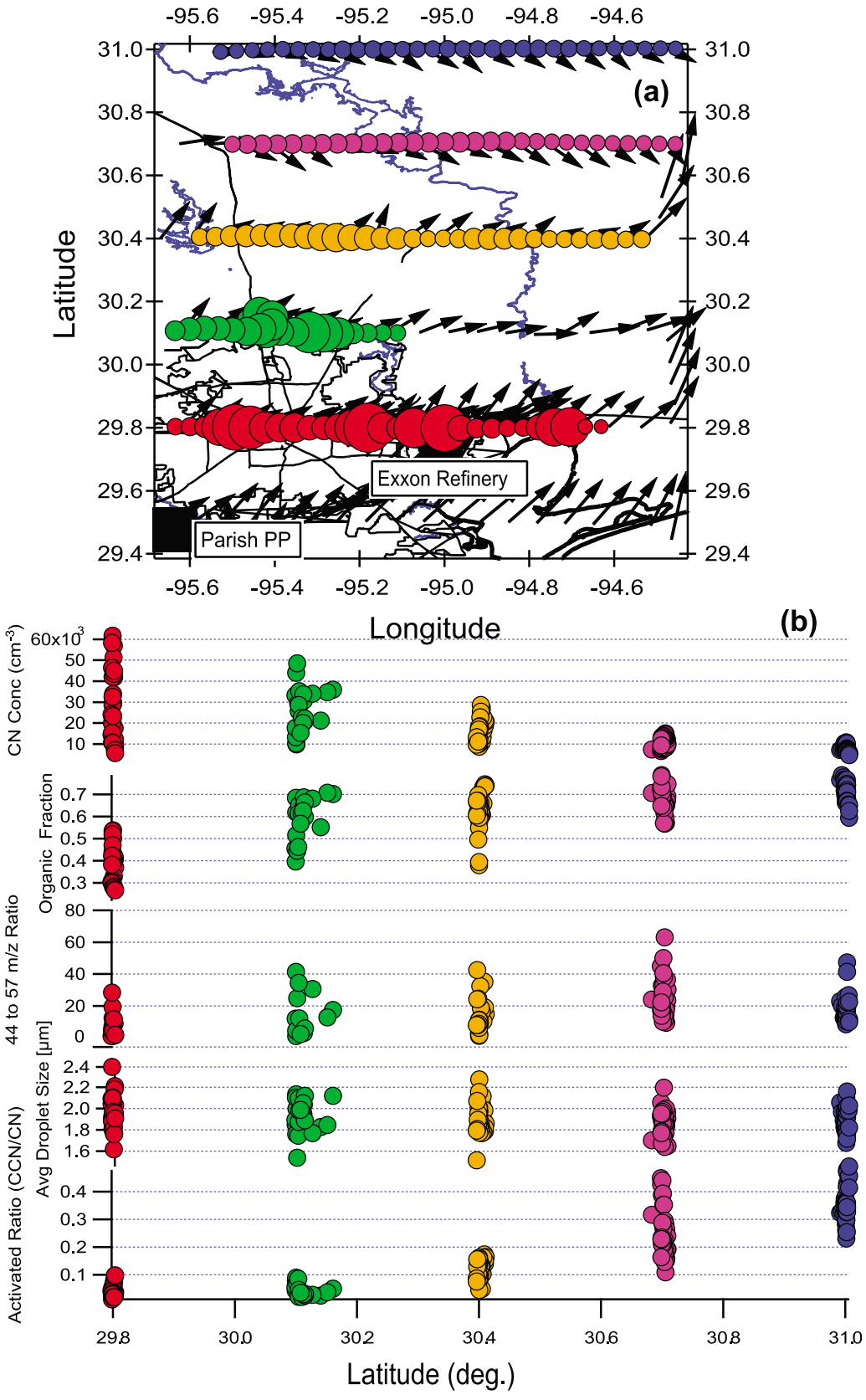

Figure 2. Research flight 2 (21 September) measurements. (a) Marker sizes reflect CN concentrations, and color corresponds to latitude of aircraft position. The separation of plumes from distinct sources is challenging; hence (b) CN concentrations, AMS spectral data, average droplet size, and activated ratio (CCN/CN) are presented for selected latitudes. Colors correspond to locations shown in Figure 2a.

those from calibration aerosol, and reflect the polydispersity of the former.

[36] The BK-INT-SOL closure scheme was best for 21 September ($S = 0.93$, $R^2 = 0.8$, $NMB = -2\%$, Table 2 and auxiliary material Figure S6b), followed by INORG ($S = 1.13$, $R^2 = 0.84$, $NMB = 15\%$, Table 2 and auxiliary material Figure S6a). Other schemes that assumed an insoluble organic component gave considerably worse closure (Table 2). In contrast to 20 September CCN predictions, 21 September INORG showed greater deviation from closure with decreasing organic fractions. *Lance et al.* [2009] observed the same type of overprediction error over the ship channel, and attributed those findings to the presence of an externally mixed aerosol strongly linked to the black carbon source. At low CCN concentrations and low organic fractions (<1500 cm^{-3} and <0.4, respectively), predictions agreed well using any of the size-invariant composition schemes (INORG, BK-INT-SOL, BK-INT, and BK-EXT; Table 2 and auxiliary material Figure S6). At larger organic fractions and CCN concentrations, BK-INT and BK-EXT underpredict CCN concentrations, while BK-INT-SOL scheme gave good closure. The results of 20 and 21 September emphasize that organics in background aerosol are partially soluble, and highlight the need for constraining the WSOC fraction, especially when organics constitute a large fraction of the aerosol mass.

4.2. Comparison of Two Metropolitan Environments

[37] On 25 September, the WP-3D aircraft headed north to Dallas and then traversed south toward the Houston metropolitan area. The daytime flight probed the mid-morning aerosol in the Dallas metropolitan area, emissions from the larger power plants in the area (Big Brown and Limestone) and the afternoon aerosol composition in the Houston metropolitan region. During this (and subsequent) flights, the CFSTGC was operated at multiple supersaturations. CCN concentrations measured throughout the day tracked the changes in total aerosol concentration; much of the aerosol were in the CCN-relevant size range, and similar to Houston were mostly composed of organics and sulfates (auxiliary material Figure S7). CCN predictions were calculated when AMS and/or PILS data where available, which for 25 September occurred during the flight leg just south of the Dallas area (between 1630 and 1930 UTC).

[38] BK-INT-SOL and INORG schemes gave the best CCN closure for both Houston and Dallas regions (Figure 3). INORG overpredicted CCN concentrations by 35% at the higher supersaturation ($s = 0.71\%$, $S = 1.352$), and 4.5% at $s = 0.43\%$ (Table 2). The BK-INT-SOL underpredicted for all s, but was best at the higher s. Relatively low R^2 suggest that either the CCN frequently deviates from a size-invariant, internally mixed composition or the size distribution varies substantially during the 40 second averaging window. BK-EXT shows substantially less scatter ($R^2 = 0.89$) than the INT schemes, but systematically underpredicts CCN concentration by a factor of 3. One can infer the nature of the aerosol mixing state from the variation in scatter (R^2) of closure agreement schemes. On 25 September, the closure schemes of this day suggest the aerosol is often externally mixed, with a size-dependent composition for each CCN population.

[39] Table 3 compares the CCN behavior of different air masses measured in the Dallas and Houston Metropolitan area on 25 September. Both regions show considerable variation in CN number yet the organic fraction in Dallas is similar to that measured in Houston (e.g., 20 and 21 September; no aerosol composition data is available in the Houston Region on 25 September). Less than 30% of the particles at the measured s act as CCN, consistent with the large number concentration of particles with diameter less than 50 nm.

4.3. CCN Characteristics of Distinct Plumes

4.3.1. Ship Channel and Houston Urban Plumes

[40] Urban and industrial plumes most often readily mix with "background" aerosol and quickly dissipate. On occasion however, plumes are distinguishable far from their source; this occurred during 26 and 27 September and 5 October (Figure 4) for emissions from downtown Houston and the ship channel. The 27th of September is characterized by the mixing of fresh urban emissions with recirculated air masses over western Houston, hence it is possible that the fresh urban plume on this day mixed with the previous day's plumes and thus appears to be more aged than the plumes originating on 27 September from the Ship Channel. The plume age and transport time was determined by the distance from ship channel and downtown center coordinates (29.776°N, 95.102°W) and (29.759°N, 95.363°W), respectively.

[41] On all 3 days, CN concentrations varied substantially within the first 5 h from emission for the ship channel center, but remained fairly constant for the downtown plume (Figure 4). Despite the difference in particle number, the organic volume fractions measured on 26 and 27 September varied between 0.7 to 0.9. The organic fraction on 5 October was less (0.5 to 0.65) which led INORG to give good closure ($S = 1.004$, $R^2 = 0.885$ for $s = 0.43\%$, and $S = 1.089$, $R^2 = 0.819$ for $s = 0.71\%$; Table 2), better than 26 and 27 September. The 5 October closure improvement was likely due to the reduced compositional variability (organic fraction) in the plumes. Including organic soluble data (BK-INT-SOL) produced similar closure results as INORG but with stronger correlation (Table 2).

[42] Organic fraction decreased with plume age on 26 September and 5 October but did not on 27 September (Figure 4). The ratio of oxygenated to less oxygenated organic aerosol on 26 September increased considerably as organic fraction decreased in the ship channel plume. This trend was consistent with an increase in CCN activation ratio, being a result of both a higher salt fraction, and larger hygroscopicity of the organic fraction (i.e., WSOC/OC). Average droplet size of activated CCN in the CFSTGC remained fairly constant throughout the measurement period (2 μm, and similar to $(NH_4)_2SO_4$ calibration droplet size). Figure 4 suggests that despite the almost immediate changes in composition and number, significant time is required (~4 h) for these changes to affect CCN concentrations in the plumes. These CCN changes can be attributed to shifts of the particle size distribution toward larger sizes, and, increases in aerosol hygroscopicity.

4.3.2. Power Plant Plumes

[43] During research flights on 26 and 27 September, the WP-3D aircraft sampled air masses in the vicinity of the Parrish power plant. On 27 September, southwesterly winds

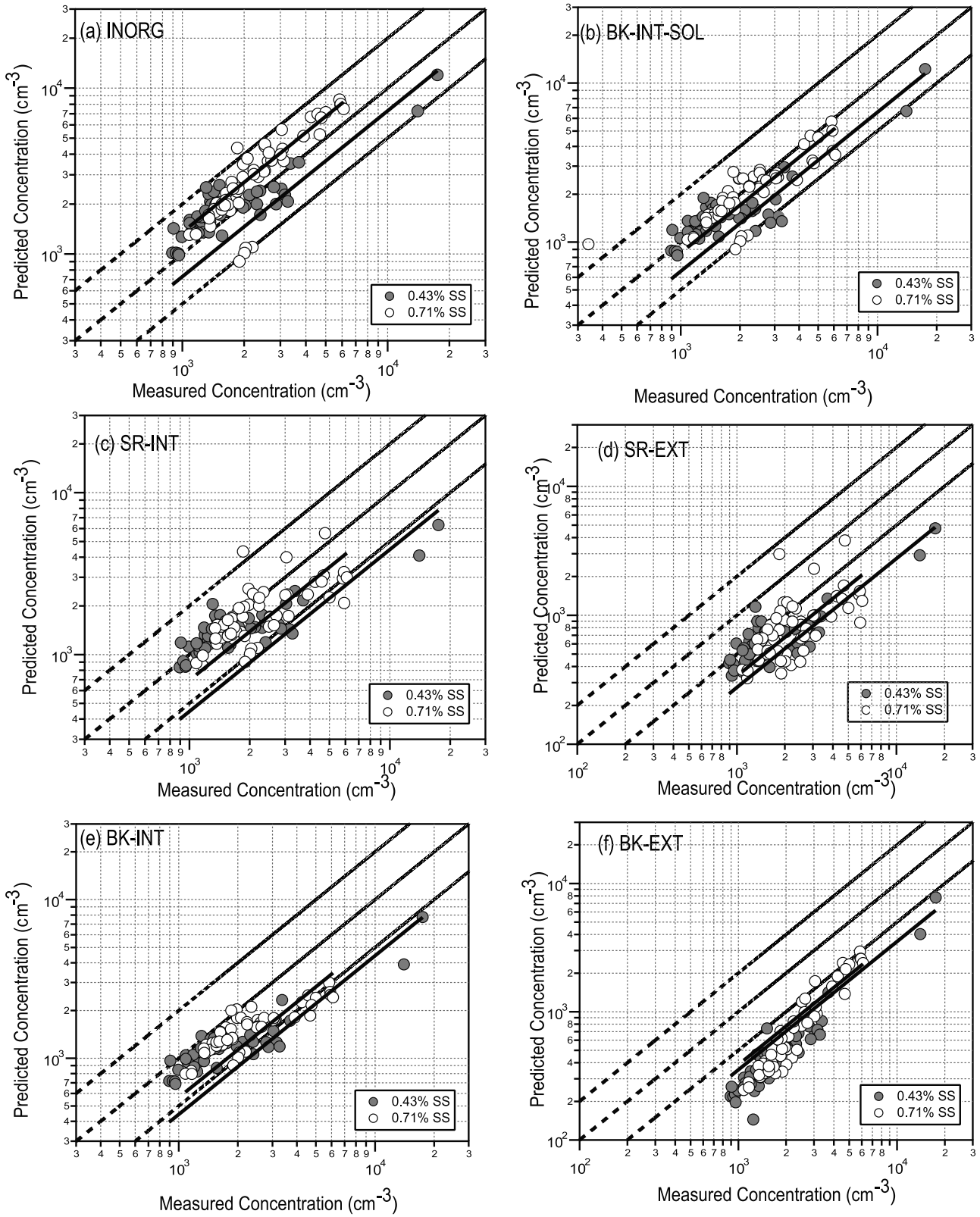

Figure 3. CCN closure plots for collected during research flight 3 (25 September), using (a) INORG, (b) BK-INT-SOL, (c) SR-INT, (d) SR-EXT, (e) BK-INT, and (f) BK-EXT schemes. Dashed lines represent 1:1 line and ±50% prediction error. Data for s = 0.43% are represented by solid symbols with a solid grey best fit line, and data for s = 0.71% are indicated with open symbols with a solid black best fit line.

Table 3. The 25 September Average Metropolitan Regional Comparison[a]

Region Studied	Dallas	Houston
Time Period, UTC	0627:15–1908:45	2016:15–2225:15
Average Total Particle Concentration (# cm^{-3})	15139 ± 14450	20753 ± 16280
Average Organic Fraction	0.79 ± 0.04	NAMS
Activated Fraction (CCN/CN) at s = 0.43%	0.14 ± 0.10	0.15 ± 0.12
Activated Fraction (CCN/CN) at s = 0.71%	0.20 ± 0.14	0.24 ± 0.15
Average Droplet Size at s = 0.43%, (μm)	1.99 ± 0.21	1.80 ± 0.26
Average Droplet Size at s = 0.71%, (μm)	2.44 ± 0.29	2.29 ± 0.24

[a]NAMS, no AMS measurements applied.

blew over the power plant toward downtown; on 26 September, northeasterly winds from downtown blew over the power plant. Hence the composition of the air mass that forms the plume may be influenced by background and urban emissions, or the combination thereof. As such, the first transect on 26 September was influenced by fresh urban emissions, whereas particulates measured in plume transects on 27 September were not (auxiliary material Figures S10 and S9). Assuming the aerosol is internally mixed on 26 September resulted in the best CCN closure (Table 2). INORG lead to significant overprediction ($NMB \geq 20\%$) which is not surprising, considering that sulfates composed $\simeq$ 30% of the aerosol volume fraction. Results from 27 September showed a similar trend, with SR-INT and BK-INT giving good and comparable closure (Table 2). On both days, the CCN closure schemes suggest that internal mixing of aerosols occurs over short spatial scales, i.e., the scale of the Houston metropolitan area (auxiliary material Figure S8 and Table 2).

4.4. Overall CCN Closure

[44] Figure 5 presents the CCN closure for all flights combined; by far, the best closure is obtained with the INORG and BK-INT-SOL schemes (Table 2). In the absence of WSOC data, INORG provides closure within 25%, with a tendency for overprediction (average S = 1.09 ± 0.13 and NMB = 11.6 ± 9.0%). The other schemes underpredicted CCN (Table 2). The variance, R^2, for the different composition schemes ranged from 0.1 to 0.5, reflective of the large variation in aerosol chemical composition, size distribution and mixing state in the data set. The sensitivity of error metrics to the closure scheme confirms that chemical composition needs to be fairly well constrained for satisfactory CCN concentration predictions. Using size-resolved and size-averaged ("bulk") chemical assumptions did equally well in obtaining closure; the internal mixing assumption gave much better closure than the external mixture model (Table 2). When organic solubility was accounted for using WSOC data and averaged thermodynamic properties, closure improved significantly compared to other organic schemes (BK-INT-SOL, average $S = 0.94 \pm 0.10$ and $NMB = -3.6 \pm 7.7\%$).

[45] The performance of BK-INT-SOL compared to the other schemes confirm the expectation that organics affect CCN activity (by depressing surface tension and contributing solute) but not as effectively as inorganic salts. The good degree of closure for the BK-INT-SOL also suggests that WSOC can be described reasonably well with a single set of hygroscopic parameters ($\frac{M}{\rho} = 1.48 \times 10^{-4}$ m^3 mol^{-1}, effective van't Hoff factor ν = 1, and 10% surface tension depression with respect to pure water hence $\kappa = 0.16$ or an effective hygroscopicity parameter of $\kappa \sim 0.3$ that assumes $\sigma = \sigma_{water}$), and knowledge of WSOC/OC is a good proxy of organic soluble fraction (hence hygroscopicity).

4.5. Hygroscopicity Parameter, κ, Analysis

[46] The generally good closure with the BK-INT-SOL scheme indicates that accounting for the hygroscopicity of the organic aerosol component is important. Figure 6 shows BK-INT-SOL scheme translated into the hygroscopicity parameter, κ, and plotted as a function of the organic fraction. Here, κ is obtained from the BK-INT-SOL predicted d_c values using equation (4). Our reported κ dependence is consistent with the previously reported values shown by *Shinozuka et al.* [2009] and *Gunthe et al.* [2009] during the MILAGRO/INTEX-B campaign over Central Mexico and the United States west coast and the AMAZE campaign in Amazonia, Brazil. As the organic mass fraction and the insoluble mass increases, κ decreases. The prescribed values of κ are = 0.6 and 0.16 for $(NH_4)_2SO_4$ and the WSOC from BK-INT-SOL, respectively. Again, κ = 0.16 for WSOC accounts for the 10% σ depression and is comparable to effective $\kappa \sim 0.3$ that assumes $\sigma = \sigma_{water}$. An upper κ limit exists for this data set (κ = 0.88) and is characterized by aerosol that is soluble like $(NH_4)_2SO_4$ but can depress surface tension up to 12% from the effect of organic surfactants. The value $\kappa \sim 0.88$ is also the value for sulfuric acid. The variability is consistent with previously reported effective κ parameter uncertainty [*Jurányi et al.*, 2009]. Effective $\kappa \sim 0.3$ has been suggested for continental aerosol hygroscopicity [e.g., *Rose et al.*, 2010; *Pringle et al.*, 2010]. The range of κ reported here expresses an average $\kappa \sim 0.3$ but with significant variability due to changes in WSOC and inorganic aerosol properties.

4.6. CCN Droplet Growth Analysis

[47] Figure 7 shows the size of activated CCN in the CFSTGC, as a function of instrument s. Using TDGA, most particles in the region showed similar kinetics to $(NH_4)_2SO_4$, with moderate growth inhibition present in only a few cases. Particles that appear to grow larger than $(NH_4)_2SO_4$ reflect the polydispersity of the aerosol size distributions. At a ground site location in Houston, *Ruehl et al.* [2008] found that up to 62% of the sampled aerosol exhibited no change in growth kinetics relative to ammonium sulfate. During the GoMACCS airborne study, *Lance et al.* [2009] found that the majority of particles activated as rapidly as $(NH_4)_2SO_4$. Our data are similar to those of *Ruehl et al.* [2008], as 60% of droplets are smaller than the threshold of rapid kinetics (Figure 7). Deconvolution of the size distribution of composition contribution to the droplet size shifts cannot be assessed solely with TDGA and will be the subject of future study.

5. Summary and Implications

[48] The aerosol in eastern Texas and the Gulf of Mexico region is primarily composed of a mixture of sulfate salts

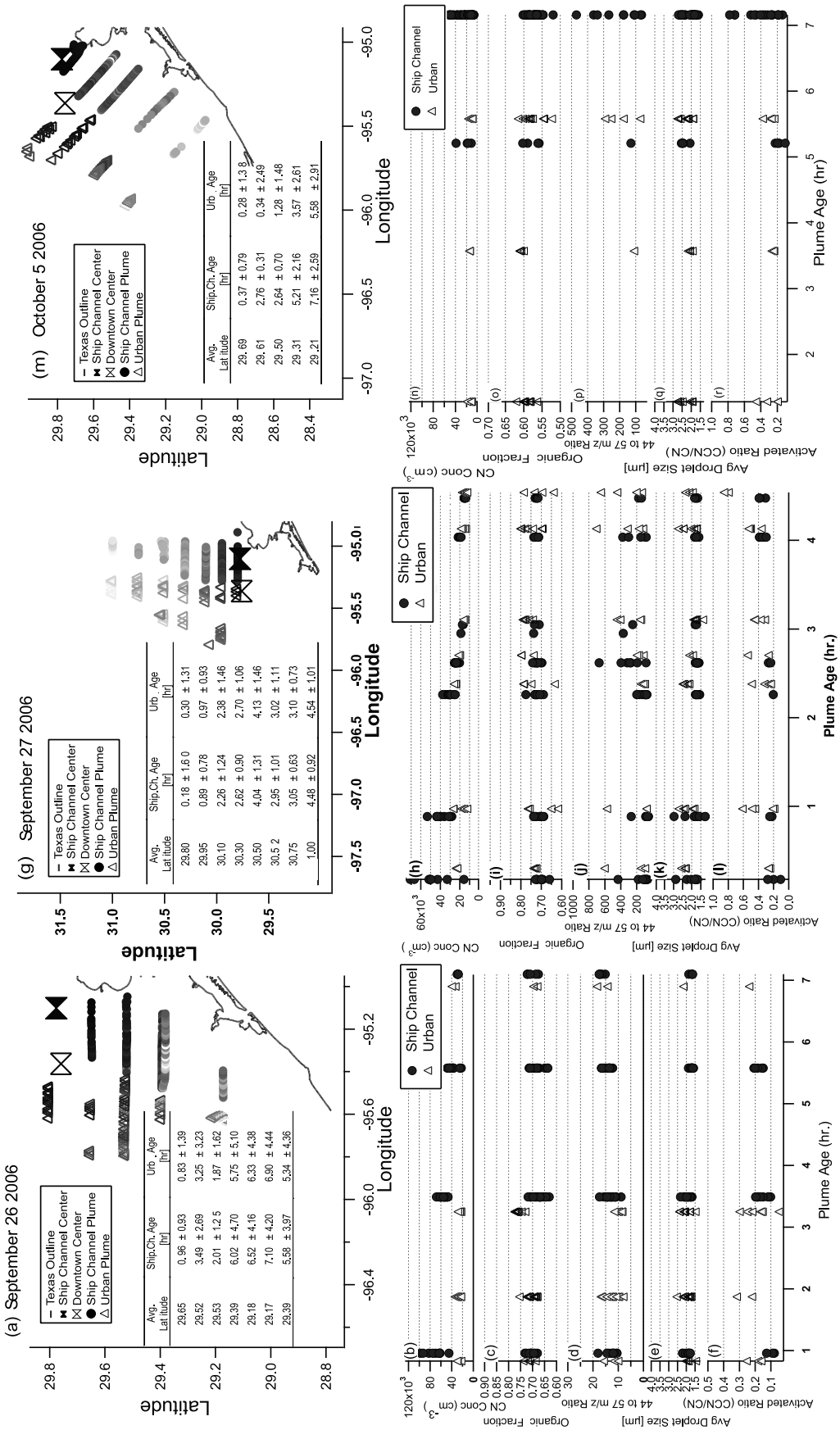

Figure 4. Urban and industrial ship channel plume analysis for (a-f) 26 September, (g-l) 27 September, and (m-r) 5 October. Emissions from downtown (open symbols) and the ship channel (solid symbols) are plotted as a function of plume age (gray scale coloring from dark to light corresponds to increasing age). Location of measurements and source centers are plotted for flights (Figures 4a, 4g, and 4l). CN concentrations (Figures 4b, 4h, and 4n), organic fraction (Figures 4c, 4i, and 4o), average droplet size (Figures 4e, 4k, and 4q), activated ratio (CCN/CN) at $s \sim 0.4\%$ (Figures 4f, 4l, and 4r), and oxygenated to less oxygenated organic AMS ratio (Figures 4d, 4j, and 4p) are plotted as a function of average plume age.

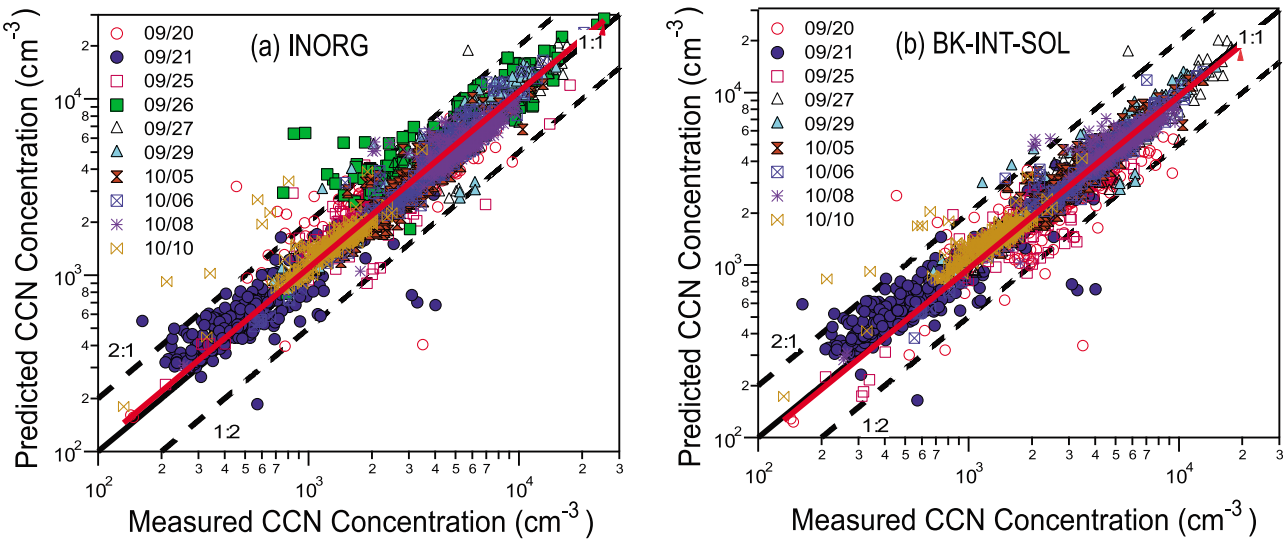

Figure 5. CCN Closure for all flights using the (a) INORG and (b) BK-INT-SOL schemes. The black solid line is the 1:1 fit, and the dashed lines represent ±50% prediction error. The solid red line represents the cumulative fit with $S = 1.11 \pm 0.09$ and $S = 0.96 \pm 0.07$ for INORG and BK-INT-SOL, respectively.

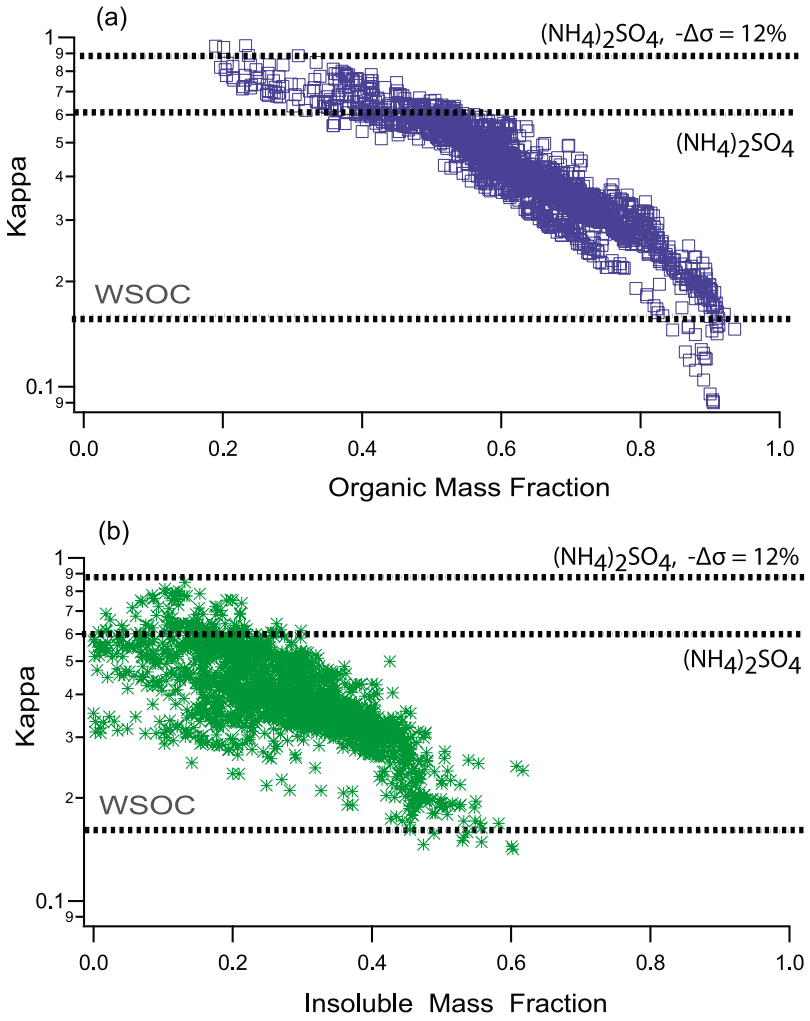

Figure 6. Inferred κ as a function of (a) organic mass fraction and (b) insoluble aerosol fraction.

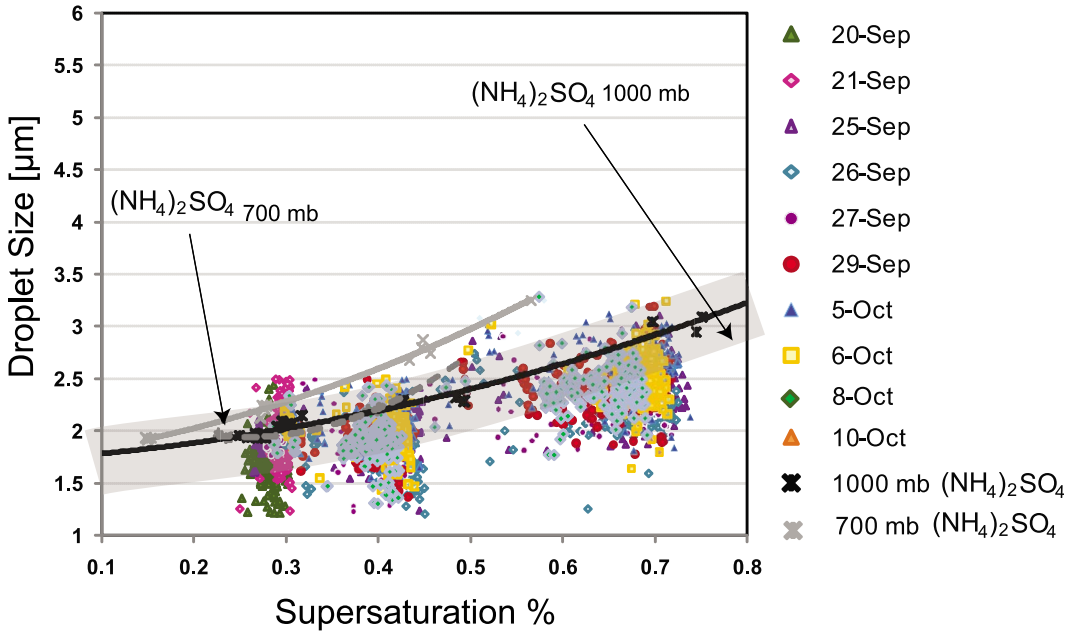

Figure 7. Droplet size data for TexAQS 2006. Droplet size as a function of instrument s. Lines represent $(NH_4)_2SO_4$ calibration measurements at different pressures, 1000 mbar (black line) and 700 mbar (grey line). The grey shaded area indicates the region of $(NH_4)_2SO_4$ droplet size variability at 1000 mbar.

and organics whose concentration and hygroscopicity change considerably with time and location. In computing CCN concentrations, assuming the aerosol is internally mixed and that a fraction of organics are soluble gives good closure; assuming that organics are completely insoluble or externally mixed with sulfates substantially worsens predictions. The closure tests considered confirm the expectation that organics are not as hygroscopic as sulfates; assuming that they are tends to overpredict CCN by as much as a factor of 2. The closure scheme that performed the best accounted for organic partial solubility and surface tension depression.

[49] Much of the aerosol contain organics in CCN relevant sizes and assuming an internal mixture gives much better closure than assuming organics are externally mixed. Close to source regions, closure error is more consistent with a less oxygenated (less hygroscopic) organic, which becomes more hygroscopic with ageing. Delays in cloud droplet growth can also be important close to source regions when organics of limited solubility constitute a substantial fraction of the aerosol volume. Quantifying and parameterizing these impacts requires a model-based deconvolution that considers CCN concentration, size polydispersity and chemical variability; this will be the subject of a future study.

[50] The average WSOC fraction is 60 ± 14% of the organic aerosol for this data set. Including the contribution of water-soluble organics to CCN activity (using the observed WSOC/OC to define the water-soluble fraction of organics with one set of WSOC hygroscopic properties obtained from independent studies) gives the best CCN closure. We postulate that the large variation in observed κ for organic species in the atmosphere can, to first order, be explained in terms of the soluble fraction in the material. Because of this, the possibility for a mechanistic, physically based prediction of hygroscopic properties of carbonaceous aerosol (namely the hygroscopicity parameter, κ) is feasible in global model assessments of the aerosol indirect effect. Given the recent and substantial amounts of available WSOC/OC data, and the treatment of the conversion process in models, it is likely that this novel set would comprehensively address the issue of predicting hygroscopic properties for organic matter in predictions of CCN.

[51] In terms of the implications of this study for global models of the aerosol indirect effect, we have shown that the assumption of internal mixture is by far the most satisfactory for computing CCN concentrations away from sources; this is because the spatial scales associated with aerosol mixing processes is at most the spatial scale of one typical global climate model grid cell (~100 km). The simplest possible assumption of chemical composition, that the material in the aerosol has the same CCN activity as sulfate salts has a tendency for overprediction that can be as much as a factor of 2. This level of uncertainty can lead to large uncertainty in indirect forcing assessments [*Sotiropoulou et al.*, 2007], especially since the largest overprediction is mostly associated with air masses where the aerosol contains a significant fraction of partially soluble organics. Unequivocally size determines particle activation more than chemistry [*Twomey*, 1977; *Dusek et al.*, 2006], but this study (among others) shows that chemical composition needs to be carefully considered as well, especially when organics constitute a large fraction of the aerosol mass. As a result, knowledge of the size-resolved soluble composition gives the best closure, in terms of bias and scatter. Finally, the degree of closure error reported here for the "best" scenario (~25%) is consistent with other published studies on CCN closure in diverse environments [e.g., *Medina et al.*, 2007; *Lance et al.*, 2009; *Quinn et al.*, 2008; *Gunthe et al.*, 2009; *Shinozuka et al.*, 2009], suggesting that the CCN prediction error in

closure studies available to date may be representative of the regional character of CCN in the North American continent.

[52] **Acknowledgments.** A.N., R.M., and A.A.A. acknowledge financial support from NOAA ACC and an NSF CAREER award. A.A.A. acknowledges support from a NASA Earth System Sciences Fellowship and a Georgia Tech FACES Postdoctoral Fellowship, while R.H.M. acknowledges support from a DOE GCEP Graduate Research Fellowship and a Georgia Tech Presidents Fellowship. We would like to thank Oscar Vargas and Phillip Walkemeyer, who aided in the integration of the CCN instrument aboard the WP-3D. P.F.D. and J.L.J. acknowledge support from NOAA (NA08OAR4310565) and EPA (FP-91650801).

References

Aiken, A. C., et al. (2008), O/C and OM/OC ratios of primary, secondary, and ambient organic aerosols with High-Resolution Time-of-Flight Aerosol Mass Spectrometry, *Environ. Sci. Technol.*, *12*, 4478–4485.

Aiken, A. C., et al. (2009), Mexico City aerosol analysis during MILAGRO using high resolution aerosol mass spectrometry at the urban supersite (T0) - Part 1: Fine particle composition and organic source apportionment, *Atmos. Chem. Phys.*, *9*, 6633–6653.

Allan, J. D., et al. (2003), Quantitative sampling using an Aerodyne aerosol mass spectrometer: 2. Measurements of fine particulate chemical composition in two U.K. cities, *J. Geophys. Res.*, *108*(D3), 4091, doi:10.1029/2002JD002359.

Allan, J. D., et al. (2004), A generalised method for the extraction of chemically resolved mass spectra from Aerodyne aerosol mass spectrometer data, *J. Aerosol Sci.*, *35*, 909–922.

Asa-Awuku, A., A. P. Sullivan, C. J. Hennigan, R. J. Weber, and A. Nenes (2008), Investigation of molar volume and surfactant characteristics of water-soluble organic compounds in biomass burning aerosol, *Atmos. Chem. Phys.*, *8*, 799–812.

Asa-Awuku, A., G. J. Engelhart, B. H. Lee, S. N. Pandis, and A. Nenes (2009), Relating CCN activity, volatility, and droplet growth kinetics of β-caryophyllene secondary organic aerosol, *Atmos. Chem. Phys.*, *9*, 795–812.

Asa-Awuku, A., A. Nenes, S. Gao, R. C. Flagan, and J. H. Seinfeld (2010), Water-soluble SOA from alkene ozonolysis: composition and droplet activation kinetics inferences from analysis of CCN activity, *Atmos. Chem. Phys.*, *10*, 1585–1597.

Bahreini, R., J. L. Jimenez, J. Wang, R. C. Flagan, J. H. Seinfeld, J. T. Jayne, and D. R. Worsnop (2003), Aircraft-based aerosol size and composition measurements during ACE-Asia using an Aerodyne aerosol mass spectrometer, *J. Geophys. Res.*, *108*(D23), 8645, doi:10.1029/2002JD003226.

Bahreini, R., E. J. Dunlea, B. M. Matthew, C. Simons, K. S. Docherty, P. F. DeCarlo, J. L. Jimenez, C. A. Brock, and A. M. Middlebrook (2008), Design and operation of a pressure-controlled inlet for airborne sampling with an aerodynamic aerosol lens, *Aerosol Sci. Technol.*, *42*, 465–471.

Bahreini, R., et al. (2009), Organic aerosol formation in urban and industrial plumes near Houston and Dallas, Texas, *J. Geophys. Res.*, *114*, D00F16, doi:10.1029/2008JD011493.

Bougiatioti, A., C. Fountoukis, N. Kalivitis, S. N. Pandis, A. Nenes, and N. Mihalopoulos (2009), Cloud condensation nuclei measurements in the marine boundary layer of the eastern Mediterranean: CCN closure and droplet growth kinetics, *Atmos. Chem. Phys.*, *9*, 7053–7066.

Brock, C. A., et al. (2008), Sources of particulate matter in the northeastern United States in summer: 2. Evolution of chemical and microphysical properties, *J. Geophys. Res.*, *113*, D08302, doi:10.1029/2007JD009241.

Broekhuizen, K., R. Y.-W. Chang, W. R. Leaitch, S. M. Li, and J. P. D. Abbatt (2006), Closure between measured and modeled cloud condensation nuclei (CCN) using size-resolved aerosol compositions in downtown Toronto, *Atmos. Chem. Phys.*, *6*, 2513–2524.

Canagaratna, M. R., et al. (2007), Chemical and microphysical characterization of ambient aerosols with the aerosol mass spectrometer, *Mass. Spectrom. Rev.*, *26*, 185–222.

Cantrell, C. A. (2008), Technical note: Review of methods for linear least-squares fitting of data and application to atmospheric chemistry problems, *Atmos. Chem. Phys.*, *8*, 5477–5487.

Cantrell, W., G. Shaw, G. R. Cass, Z. Chowdhury, L. S. Hughes, K. A. Prather, S. A. Guazzotti, and K. R. Coffee (2001), Closure between aerosol particles and cloud condensation nuclei at Kaashidhoo Climate Observatory, *J. Geophys. Res.*, *106*, 28,711–28,718, doi:10.1029/2000JD900781.

Chang, R. Y. W., P. S. K. Liu, W. R. Leaitch, and J. P. D. Abbatt (2007), Comparison between measured and predicted CCN concentrations at Egbert, Ontario: Focus on the organic aerosol fraction at a semi-rural site, *Atmos. Environ.*, *41*, 8172–8182.

Chuang, P. Y. (2003), Measurement of the timescale of hygroscopic growth for atmospheric aerosols, *J. Geophys. Res.*, *108*(D9), 4282, doi:10.1029/2002JD002757.

Clegg, S. L., and P. Brimblecombe (1988), Equilibrium partial pressures of strong acids over concentrated saline solutions - I. HNO_3, *Atmos. Environ.*, *22*, 91–100.

Conant, W. C., et al. (2004), Aerosol-cloud drop concentration closure in warm cumulus, *J. Geophys. Res.*, *109*, D13204, doi:10.1029/2003JD004324.

Covert, D. S., J. L. Gras, A. Wiedensohler, and F. Stratmann (1998), Comparison of directly measured CCN with CCN modeled from the number-size distribution in the marine boundary layer during ACE-1 at Cape Grim, Tasmania, *J. Geophys. Res.*, *103*, 16,597–16,608, doi:10.1029/98JD01093.

Cross, E. S., J. G. Slowik, P. Davidovits, J. D. Allan, D. R. Worsnop, J. T. Jayne, D. K. Lewis, M. Canagaratna, and T. B. Onasch (2007), Laboratory and ambient particle density determinations using light scattering in conjunction with aerosol mass spectrometry, *Aerosol Sci. Technol.*, *41*, 343–359.

Cubison, M., B. Ervens, G. Feingold, K. S. Docherty, I. M. Ulbrich, L. Shields, K. Prather, S. Hering, and J. L. Jimenez (2008), The influence of chemical composition and mixing state of Los Angeles urban aerosol on CCN number and cloud properties, *Atmos. Chem. Phys.*, *8*, 5649–5667.

DeCarlo, P. F., et al. (2006), A field-deployable high-resolution time-of-flight aerosol mass spectrometer, *Anal. Chem.*, *78*, 8281–8289, 2006.

Decesari, S., M. C. Facchini, M. Mircea, F. Cavalli, and S. Fuzzi (2003), Solubility properties of surfactants in atmospheric aerosol and cloud/fog water samples, *J. Geophys. Res.*, *108*(D21), 4685, doi:10.1029/2003JD003566.

Drewnick, F., et al. (2005), A new time-of-flight aerosol mass spectrometer (TOF-AMS)—Instrument description and first field deployment, *Aerosol Sci. Technol.*, *39*, 637–658.

Dusek, U., D. S. Covert, A. Wiedensohler, C. Neususs, D. Weise, and W. Cantrell (2003), Cloud condensation nuclei spectra derived from size distributions and hygroscopic properties of the aerosol in coastal south-west Portugal during ACE-2, *Tellus, Ser. B*, *55*, 35–53.

Dusek, U., et al. (2006), Size matters more than chemistry for cloud-nucleating ability of aerosol particles, *Science*, *312*, 1375–1378.

Engelhart, G., A. Asa-Awuku, A. Nenes, and S. N. Pandis (2008), CCN activity and droplet growth kinetics of fresh and aged monoterpene secondary organic aerosol, *Atmos. Chem. Phys.*, *8*, 3937–3949.

Ervens, B., M. Cubison, E. Andrews, G. Feingold, J. A. Ogren, J. L. Jimenez, E. P. DeCarlo, and A. Nenes (2007), Prediction of cloud condensation nucleus number concentration using measurements of aerosol size distributions and composition and light scattering enhancement due to humidity, *J. Geophys. Res.*, *112*, D10S32, doi:10.1029/2006JD007426.

Facchini, M., M. Mircea, S. Fuzzi, and R. Charlson (1999), Cloud albedo enhancement by surface-active organic solutes in growing droplets, *Nature*, *401*, 257–259.

Feingold, G., and P. Chuang (2002), Analysis of the influence of film-forming compounds on droplet growth: Implications for cloud microphysical processes and climate, *J. Aerosol Sci.*, *59*, 2006–2018, 2002.

Fountoukis, C., et al. (2007), Aerosol-cloud drop concentration closure for clouds sampled during (ICARTT), *J. Geophys. Res.*, *112*, D10S30, doi:10.1029/2006JD007272.

Gasparini, R., D. Collins, E. Andrews, P. Sheridan, J. Ogren, and J. Hudson (2006), Coupling aerosol size distributions and size-resolved hygroscopicity to predict humidity-dependent optical properties and cloud condensation nuclei spectra, *J. Geophys. Res.*, *111*, D05S13, doi:10.1029/2005JD006092.

Gunthe, S. S., et al. (2009), Cloud condensation nuclei in pristine tropical rainforest air of Amazonia: Size-resolved measurements and modeling of atmospheric aerosol composition and CCN activity, *Atmos. Chem. Phys.*, *9*, 7551–7575.

Haywood, J., and O. Boucher (2000), Estimates of the direct and indirect radiative forcing due to tropospheric aerosols: A review, *Rev. Geophys.*, *38*, 513–543, doi:10.1029/1999RG000078.

Hegg, D. A., D. S. Covert, H. H. Jonsson, and R. Woods (2009), Differentiating natural and anthropogenic cloud condensation nuclei in the California coastal zone, *Tellus, Ser. B*, *61*, 669–676.

Huebert, B., T. Bertram, J. Kline, S. Howell, D. Eatough, and B. Blomquist (2004), Measurements of organic and elemental carbon in Asian outflow during ACE-Asia from the NSF/NCAR C-130, *J. Geophys. Res.*, *109*, D19S11, doi:10.1029/2004JD004700.

Intergovernmental Panel on Climate Change (IPCC) (2007), Summary for policymakers, in *Climate Change (2007): The Physical Science Basis. Contribution of Working Group I to the Fourth Assessment Report of the Intergovernmental Panel on Climate Change*, pp. 1–18, Cambridge Univ. Press, Cambridge, U. K.

Ji, Q., G. E. Shaw, and W. Cantrell (1998), A new instrument for measuring cloud condensation nuclei: Cloud condensation nucleus "remover," *J. Geophys. Res.*, *103*, 28,013–28,019, doi:10.1029/98JD01884.

Jimenez, J. L., et al. (2003), Ambient aerosol sampling using the Aerodyne Aerosol Mass Spectrometer, *J. Geophys. Res.*, *108*(D7), 8425, doi:10.1029/2001JD001213.

Jimenez, J. L., et al. (2009), Evolution of organic aerosols in the atmosphere, *Science*, *326*, 1525–1529, doi:10.1126/science.1180353.

Jurányi, Z., et al. (2009), Influence of gas-to-particle partitioning on the hygroscopic and droplet activation behaviour of α-pinene secondary organic aerosol, *Phys. Chem. Chem. Phys.*, *11*, 8091–8097.

Köhler, H. (1936), The nucleus in the growth of hygroscopic droplets, *Trans. Faraday Soc.*, *43*, 1152–1161.

Kumar, P., I. N. Sokolik, and A. Nenes (2009), Parameterization of cloud droplet formation for global and regional models: including adsorption activation from insoluble CCN, *Atmos. Chem. Phys.*, *9*, 2517–2532.

Lance, S., A. Nenes, and T. A. Rissman (2004), Chemical and dynamical effects on cloud droplet number: Implications for estimates of the aerosol indirect effect, *J. Geophys. Res.*, *109*, D22208, doi:10.1029/2004JD004596.

Lance, S., J. Medina, J. N. Smith, and A. Nenes (2006), Mapping the operation of the DMT Continuous Flow CCN counter, *Aerosol Sci. Technol.*, *40*, 242–254.

Lance, S., et al. (2009), Cloud condensation nuclei activity, closure and droplet growth kinetics of Houston aerosol during the Gulf of Mexico Atmospheric Composition and Climate Study (GoMACCS), *J. Geophys. Res.*, *114*, D00F15, doi:10.1029/2008JD011699.

Lathem, T. L., and A. Nenes (2011), Water vapor depletion in the DMT continuous flow CCN chamber: Effects on supersaturation and droplet growth, *Aerosol Sci. Technol.*, *45*, 604–615.

Liu, P., W. Leaitch, C. Banic, S. Li, D. Ngo, and W. Megaw (1996), Aerosol observations at Chebogue Point during the 1993 North Atlantic Regional Experiment: Relationships among cloud condensation nuclei, size distribution, and chemistry, *J. Geophys. Res.*, *101*, 28,971–28,990, doi:10.1029/96JD00445.

Lohmann, U., and J. Feichter (2005), Global indirect aerosol effects: A review, *Atmos. Chem. Phys.*, *5*, 715–737.

Markowski, G. R. (1987), Improving Twomey algorithm for inversion of aerosol measurement data, *Aerosol Sci. Technol.*, *7*, 127–141.

McFiggans, G., et al. (2006), The effect of physical and chemical aerosol properties on warm cloud droplet activation, *Atmos. Chem. Phys.*, *6*, 2593–2649.

Medina, J., A. Nenes, R. E. P. Sotiropoulou, L. D. Cottrell, L. D. Ziemba, P. J. Beckman, and R. J. Griffin (2007), Cloud condensation nuclei closure during the International Consortium for Atmospheric Research on Transport and Transformation 2004 campaign: Effects of size-resolved composition, *J. Geophys. Res.*, *112*, D10S31, doi:10.1029/2006JD007588.

Meskhidze, N., W. L. Chameides, and A. Nenes (2005), Dust and pollution: A recipe for enhanced ocean fertilization?, *J. Geophys. Res.*, *110*, D03301, doi:10.1029/2004JD005082.

Moore, R. H., E. D. Ingall, A. Sorooshian, and A. Nenes (2008), Molar mass, surface tension, and droplet growth kinetics of marine organics from measurements of CCN activity, *Geophys. Res. Lett.*, *35*, L07801, doi:10.1029/2008GL033350.

Murphy, S., et al. (2009), Comprehensive simultaneous shipboard and airborne characterization of exhaust from a modern container ship at sea, *Environ. Sci. Technol.*, *43*, 4626–4640, doi:10.1021/es802413j.

Nenes, A., S. N. Pandis, and C. Pilinis (1998), ISORROPIA: A new thermodynamic equilibrium model for multiphase multicomponent inorganic aerosols, *Aqua. Geochem.*, *4*, 123–152.

Nenes, A., P. Y. Chuang, R. C. Flagan, and J. H. Seinfeld (2001), A theoretical analysis of cloud condensation nucleus (CCN) instruments, *J. Geophys. Res.*, *106*, 3449–3474, doi:10.1029/2000JD900614.

Nenes, A., R. J. Charlson, M. C. Facchini, M. Kulmala, A. Laaksonen, and J. H. Seinfeld (2002a), Can chemical effects on cloud droplet number rival the first indirect effect?, *Geophys. Res. Lett.*, *29*(17), 1848, doi:10.1029/2002GL015295.

Nenes, A., W. C. Conant, and J. H. Seinfeld (2002b), Black carbon radiative heating effects on cloud microphysics and implications for the aerosol indirect effect: 2. Cloud microphysics, *J. Geophys. Res.*, *107*(D21), 4605, doi:10.1029/2002JD002101.

Orsini, D. A., Y. L. Ma, A. Sullivan, B. Sierau, K. Baumann, and R. J. Weber (2003), Refinements to the particle-into-liquid sampler (PILS) for ground and airborne measurements of water soluble aerosol composition, *Atmos. Environ.*, *37*, 1243–1259.

Padró, L., A. Asa-Awuku, R. Morrison, and A. Nenes (2007), Inferring thermodynamic properties from CCN activation experiments: Single-component and binary aerosols, *Atmos. Chem. Phys.*, *7*, 5263–5274.

Padró, L. T., D. Tkacik, T. Lathem, C. J. Hennigan, A. P. Sullivan, R. J. Weber, L. G. Huey, and A. Nenes (2010), Investigation of cloud condensation nuclei properties and droplet growth kinetics of the water-soluble aerosol fraction in Mexico City, *J. Geophys. Res.*, *115*, D09204, doi:10.1029/2009JD013195.

Parrish, D. D., et al. (2009), Overview of the second Texas Air Quality Study (TexAQS II) and the Gulf of Mexico Atmospheric Composition and Climate Study (GoMACCS), *J. Geophys. Res.*, *114*, D00F13, doi:10.1029/2009JD011842.

Petters, M. D., and S. M. Kreidenweis (2007), A single parameter representation of hygroscopic growth and cloud condensation nucleus activity, *Atmos. Chem. Phys.*, *7*, 1961–1971.

Pitzer, K. S., and G. Mayorga (1973), Thermodynamics of electrolytes. II. Activity and osmotic coefficients for strong electrolytes with one or both ions univalent, *J. Phys. Chem.*, *77*, 268–277.

Prenni, A. J., M. D. Petters, S. M. Kreidenweis, P. J. DeMott, and P. J. Ziemann (2007), Cloud droplet activation of secondary organic aerosol, *J. Geophys. Res.*, *112*, D10223, doi:10.1029/2006JD007963.

Pringle, K. J., H. Tost, A. Pozzer, U. Pöschl, and J. Lelieveld (2010), Global distribution of the effective aerosol hygroscopicity parameter for CCN activation, *Atmos. Chem. Phys.*, *10*, 5241–5255.

Quinn, P. K., T. S. Bates, D. J. Coffman, and D. S. Covert (2008), Influence of particle size and chemistry on the cloud nucleating properties of aerosols, *Atmos. Chem. Phys.*, *8*, 1029–1042.

Ramanathan, V., P. J. Crutzen, J. T. Kiehl, and D. Rosenfeld (2001), Atmosphere - Aerosols, climate, and the hydrological cycle, *Science*, *294*, 2119–2124.

Rissler, J., E. Swietlicki, J. Zhou, G. Roberts, M. O. Andreae, L. Gatti, and P. Artaxo (2004), Physical properties of the sub-micrometer aerosol over the Amazon rain forest during the wet-to-dry season transition - Comparison of modeled and measured CCN concentrations, *Atmos. Chem. Phys.*, *4*, 2119–2143.

Rissman, T. A., T. M. VanReken, J. Wang, R. Gasparini, D. R. Collins, H. H. Jonsson, F. J. Brechtel, R. C. Flagan, and J. H. Seinfeld (2006), Characterization of ambient aerosol from measurements of cloud condensation nuclei during the 2003 Atmospheric Radiation Measurement Aerosol Intensive Observational Period at the Southern Great Plains site in Oklahoma, *J. Geophys. Res.*, *111*, D05S11, doi:10.1029/2004JD005695.

Roberts, G. C., and A. Nenes (2006), A continuous-flow streamwise thermal-gradient CCN chamber for atmospheric measurements, *Aerosol Sci. Technol.*, *39*, 206–221, doi:10.1080/027868290913988.

Roberts, G. C., A. Nenes, J. H. Seinfeld, and M. O. Andreae (2003), Impact of biomass burning on cloud properties in the Amazon basin, *J. Geophys. Res.*, *108*(D2), 4062, doi:10.1029/2001JD000985.

Roberts, G., G. Mauger, O. Hadley, and V. Ramanathan (2006), North American and Asian aerosols over the eastern Pacific Ocean and their role in regulating cloud condensation nuclei, *J. Geophys. Res.*, *111*, D13205, doi:10.1029/2005JD006661.

Rose, D., A. Nowak, P. Achtert, A. Wiedensohler, M. Hu, M. Shao, Y. Zhang, M. O. Andreae, and U. Pöschl (2010), Cloud condensation nuclei in polluted air and biomass burning smoke near the mega-city Guangzhou, China - Part 1: Size-resolved measurements and implications for the modeling of aerosol particle hygroscopicity and CCN activity, *Atmos. Chem. Phys.*, *10*, 3365–3383.

Ruehl, C. R., P. Y. Chuang, and A. Nenes (2008), How quickly do cloud droplets form on atmospheric particles?, *Atmos. Chem. Phys.*, *8*, 1043–1055.

Ruehl, C. R., P. Y. Chuang, and A. Nenes (2009), Distinct CCN activation kinetics above the marine boundary layer along the California coast, *Geophys. Res. Lett.*, *36*, L15814, doi:10.1029/2009GL038839.

Salcedo, D., et al. (2006), Characterization of ambient aerosols in Mexico City during the MCMA-2003 campaign with aerosol mass spectrometry: Results from the CENICA supersite, *Atmos. Chem. Phys.*, *6*, 925–946.

Schneider, J., S. Borrmann, A. G. Wollny, M. Blasner, N. Mihalopoulos, K. Oikonomou, J. Sciare, A. Teller, Z. Levin, and D. R. Worsnop (2004), Online mass spectrometric aerosol measurements during the MINOS campaign (Crete, August 2001), *Atmos. Chem. Phys.*, *4*, 65–80.

Schwarz, J. P., et al. (2006), Single-particle measurements of midlatitude black carbon and light-scattering aerosols from the boundary layer to the lower stratosphere, *J. Geophys. Res.*, *111*, D16207, doi:10.1029/2006JD007076.

Seinfeld, J. H., and S. N. Pandis (2006), *Atmospheric Chemistry and Physics: From Air Pollution to Climate Change*, John Wiley, Hoboken, N. J.

Shantz, N. C., R. Y.-W. Chang, J. G. Slowik, A. Vlasenko, J. P. D. Abbatt, and W. R. Leaitch (2010), Slower CCN growth kinetics of anthropogenic

aerosol compared to biogenic aerosol observed at a rural site, *Atmos. Chem. Phys.*, *10*, 299–312.
Shinozuka, Y., et al. (2009), Aerosol optical properties relevant to regional remote sensing of CCN activity and links to their organic mass fraction: Airborne observations over Central Mexico and the US west coast during MILAGRO/INTEX-B, *Atmos. Chem. Phys.*, *9*, 6727–6742.
Shulman, M. L., M. C. Jacobson, R. J. Carlson, R. E. Synovec, and T. E. Young (1996), Dissolution behavior and surface tension effects of organic compounds in nucleating cloud droplets, *Geophys. Res. Lett.*, *23*, 277–280, doi:10.1029/95GL03810.
Snider, J. R., and J. L. Brenguier (2000), Cloud condensation nuclei and cloud droplet measurements during ACE-2, *Tellus, Ser. B*, *52*, 828–842.
Sorooshian, A., S. Murphy, S. Hersey, H. Gates, L. Padró, A. Nenes, F. Brechtel, H. Jonsson, R. C. Flagan, and J. H. Seinfeld (2008), Comprehensive airborne characterization of aerosol from a major bovine source, *Atmos. Chem. Phys.*, *8*, 5489–5520.
Sotiropoulou, R. E. P., J. Medina, and A. Nenes (2006), CCN predictions: Is theory sufficient for assessments of the indirect effect?, *Geophys. Res. Lett.*, *33*, L05816, doi:10.1029/2005GL025148.
Sotiropoulou, R. E. P., A. Nenes, P. J. Adams, and J. H. Seinfeld (2007), Cloud condensation nuclei prediction error from application of Köhler theory: Importance for the aerosol indirect effect, *J. Geophys. Res.*, *112*, D12202, doi:10.1029/2006JD007834.
Stroud, C. A., et al. (2007), Cloud activating properties of aerosol observed during CELTIC, *J. Aerosol Sci.*, *64*, 441–459.
Sullivan, A. P., and R. J. Weber (2006), Chemical characterization of the ambient organic aerosol soluble in water: 2. Isolation of acid, neutral, and basic fractions by modified size-exclusion chromatography, *J. Geophys. Res.*, *111*, D05315, doi:10.1029/2005JD006486.
Turpin, B. J., and H. J. Lim (2001), Species contributions to PM2.5 mass concentrations: Revisiting common assumptions for estimating organic mass, *Aerosol Sci. Technol.*, *35*, 602–610.
Twomey, S. (1977), *Atmospheric Aerosols*, Elsevier Sci., Amsterdam.
VanReken, T. M., T. A. Rissman, G. C. Roberts, V. Varutbangkul, H. H. Jonsson, R. C. Flagan, and J. H. Seinfeld (2003), Toward aerosol/cloud condensation nuclei (CCN) closure during CRYSTAL-FACE, *J. Geophys. Res.*, *108*(D20), 4633, doi:10.1029/2003JD003582.
Vestin, A., J. Rissler, E. Swietlicki, G. P. Frank, and M. O. Andreae (2007), Cloud-nucleating properties of the Amazonian biomass burning aerosol: Cloud condensation nuclei measurements and modeling, *J. Geophys. Res.*, *112*, D14201, doi:10.1029/2006JD008104.
Wang, J., M. J. Cubison, A. C. Aiken, J. L. Jimenez, and D. R. Collins (2010), The importance of aerosol mixing state and size-resolved composition on CCN concentration and the variation of the importance with atmospheric aging of aerosols, *Atmos. Chem. Phys.*, *10*, 11,751–11,793.
Wilson, J. C., B. G. Lafleur, H. Hilbert, W. R. Seebaugh, J. Fox, D. W. Gesler, C. A. Brock, B. J. Huebert, and J. Mullen (2004), Function and performance of a low turbulence inlet for sampling supermicron particles from aircraft platforms, *Aerosol Sci. Technol.*, *38*, 790–802.
Wolff, G. T., M. S. Ruthosky, D. P. Stroup, and P. E. Korsog (1991), A characterization of the principal PM-10 species in Claremont (summer) and Long Beach (fall) during SCAQS, *Atmos. Environ., Part A*, *25*, 2173–2186.
Yum, S. S., G. Roberts, J. H. Kim, K. Song, and D. Kim (2006), Submicron aerosol size distributions and cloud condensation nuclei concentrations measured at Gosan, Korea, during the Atmospheric Brown Clouds-East Asian Regional Experiment 2005, *J. Geophys. Res.*, *112*, D22S32, doi:10.1029/2006JD008212.
Zappoli, S., et al. (1999), Inorganic, organic and macromolecular components of fine aerosol in different areas of Europe in relation to their water solubility, *Atmos. Environ.*, *33*, 2733–2743.
Zhang, Q., D. R. Worsnop, M. R. Canagaratna, and J. L. Jimenez (2005), Hydrocarbon-like and oxygenated organic aerosols in Pittsburgh: Insights into sources and processes of organic aerosols, *Atmos. Chem. Phys.*, *5*, 3289–3311.
Zhang, Q., J. L. Jimenez, D. R. Worsnop, and M. Canagaratna (2007), A case study of urban particle acidity and its influence on secondary organic aerosol, *Environ. Sci. Technol.*, *41*, 3213–3219.

A. Asa-Awuku, Department of Chemical and Environmental Engineering, Bourns College of Engineering-Center for Environmental Research and Technology, University of California, Riverside, CA 92507, USA. (akua@engr.ucr.edu)

R. Bahreini, C. A. Brock, J. S. Holloway, A. M. Middlebrook, and T. B. Ryerson, Chemical Sciences Division, Earth System Research Laboratory, National Oceanic and Atmospheric Administration, Boulder, CO 80305, USA.

P. F. DeCarlo and J. L. Jimenez, Cooperative Institute for Research in Environmental Sciences, University of Colorado at Boulder, Boulder, CO 80309, USA.

A. Hecobian, L. G. Huey, A. Nenes, R. Stickel, D. J. Tanner, and R. J. Weber, School of Earth and Atmospheric Sciences, Georgia Institute of Technology, Atlanta, GA 30332, USA.

R. H. Moore, School of Chemical and Biomolecular Engineering, Georgia Institute of Technology, Atlanta, GA 30332, USA.